

One-loop contributions for $A^0 \rightarrow \ell\bar{\ell}V$ with $\ell \equiv e, \mu$ and $V \equiv \gamma, Z$ in Higgs Extensions of the Standard Model

Khiem Hong Phan^{a,b}, Dzung Tri Tran^{a,b}, Thanh Huy Nguyen^c

^a*Institute of Fundamental and Applied Sciences, Duy Tan University, Ho Chi Minh City 700000, Vietnam*

^b*Faculty of Natural Sciences, Duy Tan University, Da Nang City 550000, Vietnam*

^c*VNUHCM-University of Science, 227 Nguyen Van Cu, District 5, Ho Chi Minh City 700000, Vietnam*

Abstract

We present one-loop formulas for the decay of CP-odd Higgs $A^0 \rightarrow \ell\bar{\ell}V$ with $\ell \equiv e, \mu$ and $V \equiv \gamma, Z$ in Higgs Extensions of the Standard Model, considering two higgs doublet model with a complex (and real) scalar, two higgs doublet model as well as triplet higgs model. Analytic results for one-loop amplitudes are expressed in terms of Passarino-Veltman functions following the standard notations of `LoopTools`. As a result, physical results can be generated numerically by using the package. In phenomenological results, the total decay widths and the differential decay rates with respect to the invariant mass of lepton pair are analyzed for two typical models such as two higgs doublet model and triplet higgs model.

Keywords: Higgs phenomenology, One-loop Feynman integrals, Analytic methods for Quantum Field Theory, Dimensional regularization, Future lepton colliders.

1. Introduction

Discovering the scalar Higgs potential, subsequently answering the nature of dynamic of the electroweak spontaneous symmetry breaking (EWSB), is one of the priority tasks at future colliders, e.g. High-luminosity Large Hadron Collider (HL-LHC) [1, 2] as well as future Lepton Colliders (LC) [3]. It is well-known that the scalar potential is extended by including scalar singlets or scalar multiplets in many of beyond the standard models (BSM). As a result, there exist many new heavy scalar particles, for examples, neutral CP-even and CP-odd Higgses, singly charged Higgses as well as doubly charged Higgses in many of BSMs. The precise measurements for decay widths and the production cross-sections of the scalar particles are important for the indirect and direct searches for new physic signals at future colliders. From the measured data, we can therefore verify the nature of scalar Higgs potential and understand deeply the dynamic of EWSB. Recently, direct production of a light CP-odd Higgs boson has been performed at the Tevatron and LHC [4], search for a CP-odd Higgs boson decaying to Zh in pp collisions has performed at the LHC [5, 6]. Probing for a light pseudoscalar Higgs boson in $\mu\mu\tau\tau$ events at the LHC in [7] and in the di-muon decay channels in pp collisions at $\sqrt{s} = 7$ TeV [8] has reported.

From theoretical views, the detailed evaluations for one-loop radiative corrections to the decay rates and the production cross-sections for the standard model-like Higgs boson (SM-like Higgs) as well as for all new scalar particles in many of BSMs play a crucial role for probing new physics signals at future colliders. One-loop contributing to the decay and production processes of SM-like Higgs, CP-even Higgses have computed in many Higgs Extensions of the SM (HESM). It is worth to refer to typical works in this paper, for examples, in the works of

Email address: phanhongkhiem@duytan.edu.vn (Khiem Hong Phan)

following papers [9, 10, 11, 12, 13, 14, 15, 16, 17, 18, 19, 20, 21] and the references therein. One-loop radiative corrections to the CP-odd Higgs (A^0) production processes in the HESM have evaluated at LHC [22, 23, 24] and at future LC [25, 26, 27, 28]. Furthermore, the decay channels of the CP-odd Higgs including one-loop and beyond one-loop corrections have also computed in many of BSMs as in [29, 30, 31, 32, 33, 34]. In this work, we present the first calculations of one-loop contributing for decay channels $A^0 \rightarrow \ell\bar{\ell}V$ with $\ell \equiv e, \mu$ and $V \equiv \gamma, Z$ within many of HESM frameworks, including two higgs doublet model with a complex (and real) scalar, two higgs doublet model as well as triplet higgs model. Analytic results for one-loop form factors are expressed in terms of Passarino-Veltman scalar functions (PV-functions) following the standard notations of `LoopTools` [35]. Subsequently, physical results can be computed numerically by using the package. In phenomenological results, the decay rates of CP-odd Higgs and its differential decay widths with respect to the invariant mass of lepton pair are examined for two typical models such as two higgs doublet model (THDM) and triplet higgs model (THM).

Overview of the paper is as follows. We first review two specific classifications of HESMs in detail in this work such as two higgs doublet model with a complex scalar field and triplet higgs model in the section 2. We then present in concrete the evaluations for one-loop contributions to the decay amplitudes $A^0 \rightarrow \ell\bar{\ell}V$ in the section 3. Phenomenological results for the HESMs are shown in section 4. Conclusion and outlook are devoted in section 5. In appendices *A, B* we derive all related couplings to the processes under consideration in the above-mentioned models. Proving one-loop mixings of A^0 with scalar CP-even Higgs ϕ , of with Z boson as well as the mixings of ϕ with Z boson are vanished in appendices *C, D*.

2. Higgs Extension Standard Models

In this section, we review the Higgs Extensions of the Standard Models, examining two higgs doublet model with a complex scalar field (noted as THDMS, or STHDM hereafter) [36], with soft breaking Z_2 symmetry and triplet higgs models. From the general STHDM, we can reduce to the next minimum two higgs doublet models (NTHDM) [37, 38] and THDM [39, 40, 41, 42, 43, 45, 46, 47]. We then turn our attention to the second classification of HESM, triplet higgs model (THM), in the subsection 2.2.

2.1. STHDM

In this subsection, we arrive at STHDM, the two higgs doublet model with adding a complex scalar field S , following the soft breaking Z_2 symmetry. In this model, two scalar fields Φ_1 and Φ_2 are doublets of $SU(2)_L$ with hypercharge $Y = +1/2$. The additional complex scalar S is a scalar singlet of $SU(2)_L$ with with hypercharge $Y = 0$. In this paper, we only concern the CP-conserving case for the scalar sector. As a result, all parameters in scalar potential are considered to be real parameters. Furthermore, the scalar potential follows the soft breaking term of Z_2 symmetry, e.g. $\Phi_i \rightarrow -\Phi_i$ for $i = 1, 2$. Under the above assumptions, the most generalized gauge invariant formulation in accordance with the renormalizable condition for the

scalar potential is given by:

$$\begin{aligned}
\mathcal{V}_{\text{STHDM}} = & m_{11}^2 |\Phi_1|^2 + m_{22}^2 |\Phi_2|^2 - m_{12}^2 (\Phi_1^\dagger \Phi_2 + \Phi_2^\dagger \Phi_1) + \frac{\lambda_1}{2} |\Phi_1|^4 + \frac{\lambda_2}{2} |\Phi_2|^4 \\
& + \lambda_3 |\Phi_1|^2 |\Phi_2|^2 + \lambda_4 |\Phi_1^\dagger \Phi_2|^2 + \frac{\lambda_5}{2} [(\Phi_1^\dagger \Phi_2)^2 + (\Phi_2^\dagger \Phi_1)^2] \\
& - m_S^2 |S|^2 + \frac{\lambda_S}{2} |S|^4 + \lambda_{S\Phi_1} |\Phi_1|^2 |S|^2 + \lambda_{S\Phi_2} |\Phi_2|^2 |S|^2 \\
& + \left\{ -\frac{m_S'^2}{4} S^2 + \text{H.c.} \right\}.
\end{aligned} \tag{1}$$

The potential includes a scalar sector from THDM, a singlet complex Higgs part and the mixing term of THDM with singlet complex scalar S . In the above scalar potential, the last term is broken softly the $U(1)$ symmetry.

For the electroweak spontaneous symmetry breaking, the scalar fields can be parameterized as follows:

$$\Phi_1 = \begin{pmatrix} \phi_1^+ \\ (v_1 + \rho_1 + i\eta_1)/\sqrt{2} \end{pmatrix}, \quad \Phi_2 = \begin{pmatrix} \phi_2^+ \\ (v_2 + \rho_2 + i\eta_2)/\sqrt{2} \end{pmatrix}, \quad S = \frac{v_s + \rho_3 + i\chi}{\sqrt{2}}. \tag{2}$$

By minimizing the potential, we find the following system equations:

$$m_{11}^2 = \frac{v_2}{v_1} m_{12}^2 - \frac{1}{2} \lambda_1 v_1^2 - \frac{1}{2} \lambda_{345} v_2^2 - \frac{1}{2} \lambda_{S\Phi_1} v_s^2, \tag{3}$$

$$m_{22}^2 = \frac{v_1}{v_2} m_{12}^2 - \frac{1}{2} \lambda_2 v_2^2 - \frac{1}{2} \lambda_{345} v_1^2 - \frac{1}{2} \lambda_{S\Phi_2} v_s^2, \tag{4}$$

$$m_S^2 = -\frac{1}{2} m_S'^2 + \frac{1}{2} \lambda_S v_s^2 + \frac{1}{2} \lambda_{S\Phi_1} v_1^2 + \frac{1}{2} \lambda_{S\Phi_2} v_2^2, \tag{5}$$

where the notation $\lambda_{ijk\dots} = \lambda_i + \lambda_j + \lambda_k + \dots$ has used. In this model, χ becomes a stable dark matter (DM) candidate. After the EWSB, the mass of χ is given by:

$$m_\chi^2 = m_S^2 = -m_S^2 + \frac{1}{2} m_S'^2 + \frac{1}{2} \lambda_S v_s^2 + \frac{1}{2} \lambda_{S\Phi_1} v_1^2 + \frac{1}{2} \lambda_{S\Phi_2} v_2^2. \tag{6}$$

In scenario of $m_S'^2 = 0$, it means there isn't soft breaking term in this case. As a result, χ becomes a massless Nambu-Goldstone boson. For the case of $m_S'^2 > 0$, χ has non-zero mass, χ is a pseudo-Nambu-Goldstone boson. In the scope of this paper, the role of χ isn't related to the processes under concern. Therefore, we skip discussing χ in the rest of this paper.

The charged scalars part can be collected in the form of

$$\mathcal{L}_{\text{mass}}^{\phi^\pm} = - \left(m_{12}^2 - \frac{1}{2} \lambda_{45} v_1 v_2 \right) (\phi_1^-, \phi_2^-) \begin{pmatrix} v_2/v_1 & -1 \\ -1 & v_1/v_2 \end{pmatrix} \begin{pmatrix} \phi_1^+ \\ \phi_2^+ \end{pmatrix}. \tag{7}$$

The CP -odd scalar sector is presented as the same form as follows:

$$\mathcal{L}_{\text{mass}}^\eta = -\frac{1}{2} (m_{12}^2 - \lambda_5 v_1 v_2) (\eta_1, \eta_2) \begin{pmatrix} v_2/v_1 & -1 \\ -1 & v_1/v_2 \end{pmatrix} \begin{pmatrix} \eta_1 \\ \eta_2 \end{pmatrix}. \tag{8}$$

Physical mass terms can be obtained by diagonalizing the above matrices. This can be done by applying the following rotation matrices:

$$\begin{pmatrix} \phi_1^+ \\ \phi_2^+ \end{pmatrix} = R(\beta) \begin{pmatrix} G^+ \\ H^+ \end{pmatrix}, \quad \begin{pmatrix} \eta_1 \\ \eta_2 \end{pmatrix} = R(\beta) \begin{pmatrix} G^0 \\ A^0 \end{pmatrix}, \quad R(\beta) = \begin{pmatrix} c_\beta & -s_\beta \\ s_\beta & c_\beta \end{pmatrix}, \tag{9}$$

where the rotation angle β is given by:

$$t_\beta = \frac{v_2}{v_1}. \quad (10)$$

We know that G^\pm and G^0 are being massless Nambu-Goldstone bosons giving the masses for the weak gauge bosons W^\pm and Z , respectively. The remaining physical states H^\pm and A^0 become charged Higgs and CP-odd Higgs. Their masses are then given by

$$M_{H^\pm}^2 = \frac{v_1^2 + v_2^2}{v_1 v_2} \left[m_{12}^2 - \frac{1}{2} \lambda_{45} v_1 v_2 \right], \quad (11)$$

$$M_{A^0}^2 = \frac{v_1^2 + v_2^2}{v_1 v_2} (m_{12}^2 - \lambda_5 v_1 v_2). \quad (12)$$

As the same procedure, the CP -even scalars ρ_1 , ρ_2 , and ρ_3 can be first collected in the form of

$$\mathcal{L}_{\text{mass}}^\rho = -\frac{1}{2} (\rho_1, \rho_2, \rho_3) \mathcal{M}_\rho^2 \begin{pmatrix} \rho_1 \\ \rho_2 \\ \rho_3 \end{pmatrix}. \quad (13)$$

Where the elements of the matrix \mathcal{M}_ρ^2 are shown as follows:

$$(\mathcal{M}_\rho^2)_{11} = \lambda_1 v_1^2 + \frac{v_2}{v_1} m_{12}^2, \quad (\mathcal{M}_{\rho_s}^2)_{22} = \lambda_2 v_2^2 + \frac{v_1}{v_2} m_{12}^2, \quad (14)$$

$$(\mathcal{M}_\rho^2)_{33} = \lambda_S v_s^2, \quad (\mathcal{M}_\rho^2)_{12} = \lambda_{345} v_1 v_2 - m_{12}^2, \quad (15)$$

$$(\mathcal{M}_\rho^2)_{13} = \lambda_{S\Phi_1} v_1 v_s, \quad (\mathcal{M}_\rho^2)_{23} = \lambda_{S\Phi_2} v_2 v_s. \quad (16)$$

The matrix \mathcal{M}_ρ^2 can be diagonalized by applying the rotation matrix \mathcal{O} as follows:

$$\text{diag}(M_{H_1}^2, M_{H_2}^2, M_{H_3}^2) = \mathcal{O}^T \mathcal{M}_\rho^2 \mathcal{O}. \quad (17)$$

As a result, the mass eigenstates H_i are then related to the flavor bases ρ_i for $i = 1, 2, 3$ via the rotation matrix \mathcal{O} as

$$\begin{pmatrix} \rho_1 \\ \rho_2 \\ \rho_3 \end{pmatrix} = \mathcal{O} \begin{pmatrix} H_1 \\ H_2 \\ H_3 \end{pmatrix}. \quad (18)$$

Detail the form of \mathcal{O} is given explicitly in Appendix A. Finally, we get the physical masses CP-even Higgses. One of H_i becomes the SM-like Higgs boson. In this paper, we note that h^0 is the SM-like Higgs boson and H_j for remaining CP-even Higgses in the model under consideration for the later computation.

We turn our attention to kinetic terms of the above Lagrangian. The terms are expressed as follows:

$$\mathcal{L}_{\text{kin}} = (D^\mu \Phi_1)^\dagger D_\mu \Phi_1 + (D^\mu \Phi_2)^\dagger D_\mu \Phi_2. \quad (19)$$

Masses for the weak gauge bosons can be derived from expanding the kinetic terms. In detail, mass terms can be collected in the form of

$$\mathcal{L}_{\text{mass}}^V = \frac{g^2}{4} (v_1^2 + v_2^2) W^{-,\mu} W_\mu^+ + \frac{1}{2} \frac{g^2}{4c_W^2} (v_1^2 + v_2^2) Z^\mu Z_\mu. \quad (20)$$

Here, we use $c_W = \cos \theta_W$ which is cosine of Weinberg's angle. In this equation, we fix $v = \sqrt{v_1^2 + v_2^2} \sim 246$ GeV at electroweak scale. The masses of W and Z bosons then read

$$M_W = \frac{gv}{2}, \quad M_Z = \frac{gv}{2c_W}. \quad (21)$$

Finally, we consider the Yukawa sector. In order to avoid Tree-level Flavor-Changing Neutral Currents (FCNCs), four independent types of Yukawa couplings are listed as follows:

$$\text{Type I: } \mathcal{L}_Y^{(I)} = -y_{\ell_i} \bar{L}_{iL} \ell_{iR} \Phi_2 - \tilde{y}_d^{ij} \bar{Q}_{iL} d'_{jR} \Phi_2 - \tilde{y}_u^{ij} \bar{Q}_{iL} u'_{jR} \tilde{\Phi}_2 + \text{H.c.} \quad (22)$$

$$\text{Type II: } \mathcal{L}_Y^{(II)} = -y_{\ell_i} \bar{L}_{iL} \ell_{iR} \Phi_1 - \tilde{y}_d^{ij} \bar{Q}_{iL} d'_{jR} \Phi_1 - \tilde{y}_u^{ij} \bar{Q}_{iL} u'_{jR} \tilde{\Phi}_2 + \text{H.c.} \quad (23)$$

$$\text{Type X: } \mathcal{L}_Y^{(X)} = -y_{\ell_i} \bar{L}_{iL} \ell_{iR} \Phi_1 - \tilde{y}_d^{ij} \bar{Q}_{iL} d'_{jR} \Phi_2 - \tilde{y}_u^{ij} \bar{Q}_{iL} u'_{jR} \tilde{\Phi}_2 + \text{H.c.} \quad (24)$$

$$\text{Type Y: } \mathcal{L}_Y^{(Y)} = -y_{\ell_i} \bar{L}_{iL} \ell_{iR} \Phi_2 - \tilde{y}_d^{ij} \bar{Q}_{iL} d'_{jR} \Phi_1 - \tilde{y}_u^{ij} \bar{Q}_{iL} u'_{jR} \tilde{\Phi}_2 + \text{H.c.} \quad (25)$$

Here $\tilde{\Phi}_2 = i\sigma^2 \Phi_2^*$, lepton doublet $L_{iL} = (\nu_{iL}, \ell_{iL})^T$ for generation index $i = 1, 2, 3$ and quark doublet $Q_{iL} = (u'_{iL}, d'_{iL})^T$. The mixing matrices \tilde{y}_d^{ij} for down-quarks and \tilde{y}_u^{ij} for up-quarks can be diagonalized by following rotation matrix $(U_d)_{ij}$. In detail, we have

$$(U_d)_{ij}^\dagger \tilde{y}_d^{jk} (U_d)_{kl} = y_{d_i} \delta_{il}, \quad (26)$$

$$(U_u)_{ij}^\dagger \tilde{y}_u^{jk} (U_u)_{kl} = y_{u_i} \delta_{il}. \quad (27)$$

The quarks basis u'_i and d'_i are related to their mass basis u_i and d_i through

$$d'_i = (U_d)_{ij} d_j, \quad u'_i = (U_u)_{ij} u_j. \quad (28)$$

The Cabibbo-Kobayashi-Maskawa matrix is then identified as

$$\text{CKM}_{ij} = (U_u)_{ik}^\dagger (U_d)_{kj}. \quad (29)$$

Since we aren't interested in neutrino physics in this work, we assume the lepton sector is the same as in the SM. After the EWSB, the four types of Yukawa interactions can be written in the form of

$$\mathcal{L}_Y \supset - \sum_{f=\ell_j, d_j, u_j} \left[m_f \bar{f} f + \sum_{i=1}^3 \kappa_{H_i}^f \frac{m_f}{v} H_i \bar{f} f + \kappa_{A^0}^f \frac{m_f}{v} A^0 \bar{f} i \gamma_5 f \right]. \quad (30)$$

The couplings of H_i and A_0 to fermion pair are taken the form of

$$g_{H_i f \bar{f}} = -\kappa_{H_i}^f \frac{m_f}{v}, \quad g_{A_0 f \bar{f}} = -i \kappa_{A^0}^f \frac{m_f}{v} \gamma_5. \quad (31)$$

The coefficients $\kappa_{H_i}^f$ and $\kappa_{A^0}^f$ are shown in detail in Table 1. Here we note h^0 is SM-like Higgs boson and H_j for new heavy CP-even Higgses in the corresponding models in the following Table.

κ -factors	Type I	Type II	Type X	Type Y
$\kappa_{H_i}^{\ell_j}$	\mathcal{O}_{2i}/s_β	\mathcal{O}_{1i}/c_β	\mathcal{O}_{1i}/c_β	\mathcal{O}_{2i}/s_β
$\kappa_{H_i}^{d_j}$	\mathcal{O}_{2i}/s_β	\mathcal{O}_{1i}/c_β	\mathcal{O}_{2i}/s_β	\mathcal{O}_{1i}/c_β
$\kappa_{H_i}^{u_j}$	\mathcal{O}_{2i}/s_β	\mathcal{O}_{2i}/s_β	\mathcal{O}_{2i}/s_β	\mathcal{O}_{2i}/s_β
$\kappa_{A^0}^{\ell_j}$	$1/t_\beta$	$-t_\beta$	$-t_\beta$	$1/t_\beta$
$\kappa_{A^0}^{d_j}$	$1/t_\beta$	$-t_\beta$	$1/t_\beta$	$-t_\beta$
$\kappa_{A^0}^{u_j}$	$-1/t_\beta$	$-1/t_\beta$	$-1/t_\beta$	$-1/t_\beta$

Table 1: The factors $\kappa_{H_i}^f$ and $\kappa_{A^0}^f$ are listed for four types of STHDM. The elements of the rotation matrix \mathcal{O}_{ij} are given explicitly in Appendices A, B. It is noted that h^0 is noted for the SM-like Higgs boson and H_j are for remaining CP-even Higgses in the mentioned models.

Other couplings relating to the processes under consideration are listed in Table 2. In the Table 2, a general form of the couplings are shown in the second column. In the third column, we present the couplings in STHDM. While the couplings in THDM can be reduced from the third column and are presented in the last column. For the vertices of scalar particle with vector boson pair, we express the couplings in terms of κ -factor of the SM's couplings. The couplings for SM-like Higgs to vector boson pair in the SM are given $g_{h^0ZZ}^{\text{SM}} = \frac{eM_W}{c_W^2 s_W}$, $g_{h^0WW}^{\text{SM}} = \frac{eM_W}{s_W}$.

Vertices	HESM	STHDM	THDM
$A^0 Z_\mu \phi$	$g_{A^0 Z h^0} \cdot (p^{h^0} - p^{A^0})^\mu$	$\frac{e}{s_{2W}} (-s_\beta \mathcal{O}_{12} + c_\beta \mathcal{O}_{22}) \cdot (p^{h^0} - p^{A^0})^\mu$	$\frac{e c_{\beta-\alpha}}{s_{2W}} (p^{h^0} - p^{A^0})^\mu$
	$g_{A^0 Z H_j} \cdot (p^{H_j} - p^{A^0})^\mu$	$\frac{-e}{s_{2W}} (c_\beta \mathcal{O}_{2j} - \mathcal{O}_{1j} s_\beta) \cdot (p^{H_j} - p^{A^0})^\mu$	$\frac{-e s_{\beta-\alpha}}{s_{2W}} (p^H - p^{A^0})^\mu$
$\phi Z_\mu Z_\nu$	$-i \kappa_{h^0 ZZ} \cdot g_{h^0 ZZ}^{\text{SM}} \cdot g^{\mu\nu}$	$-i [c_\beta \mathcal{O}_{11} + s_\beta \mathcal{O}_{21}] \cdot g_{h^0 ZZ}^{\text{SM}} \cdot g^{\mu\nu}$	$i s_{\beta-\alpha} \cdot g_{h^0 ZZ}^{\text{SM}} \cdot g^{\mu\nu}$
	$-i \kappa_{H_j ZZ} \cdot g_{h^0 ZZ}^{\text{SM}} \cdot g^{\mu\nu}$	$-i [c_\beta \mathcal{O}_{1j} + s_\beta \mathcal{O}_{2j}] \cdot g_{h^0 ZZ}^{\text{SM}} \cdot g^{\mu\nu}$	$i c_{\beta-\alpha} \cdot g_{h^0 ZZ}^{\text{SM}} \cdot g^{\mu\nu}$
$\phi W_\mu^\pm W_\nu^\mp$	$-i \kappa_{h^0 WW} \cdot g_{h^0 WW}^{\text{SM}} \cdot g^{\mu\nu}$	$-i [c_\beta \mathcal{O}_{11} + s_\beta \mathcal{O}_{21}] \cdot g_{h^0 WW}^{\text{SM}} \cdot g^{\mu\nu}$	$i s_{\beta-\alpha} \cdot g_{h^0 WW}^{\text{SM}} \cdot g^{\mu\nu}$
	$-i \kappa_{H_j WW} \cdot g_{h^0 WW}^{\text{SM}} \cdot g^{\mu\nu}$	$-i [c_\beta \mathcal{O}_{1j} + s_\beta \mathcal{O}_{2j}] \cdot g_{h^0 WW}^{\text{SM}} \cdot g^{\mu\nu}$	$i c_{\beta-\alpha} \cdot g_{h^0 WW}^{\text{SM}} \cdot g^{\mu\nu}$

Table 2: All related couplings with $V \equiv \gamma, Z$ and $\phi \equiv h^0, H_j$ to the processes under consideration. H_j is for remaining CP-even Higgses in the mentioned models. Here, we have the SM couplings as $g_{h^0 ZZ}^{\text{SM}} = \frac{eM_W}{c_W^2 s_W}$, $g_{h^0 WW}^{\text{SM}} = \frac{eM_W}{s_W}$. In THDM, one has $H_j = H$ and we have the appropriate couplings in the last column.

We note that we can derive the corresponding couplings for NTHDM by considering the singlet scalar S being real scalar field. In order to arrive at the respective couplings in THDM, we take the limits for the rotation matrix \mathcal{O} in Appendix A as follows: $c_{12} \rightarrow c_\alpha$ and $s_{23} = s_{13} = 0$.

2.2. Triplet Higgs Models

We turn our attention to another type of the HESM which is triplet higgs model (THM), a classification of the SM with adding a real Higgs triplet, denoted as Δ with hypercharge $Y_\Delta = 2$ [48, 49, 50, 51, 52, 53, 54, 55, 56, 57, 58, 59, 61, 62, 63]. The most general form of the scalar potential of THM with obeying the renormalizable condition and the gauge invariance is taken the form of:

$$\begin{aligned} \mathcal{V}_{THM}(\Phi, \Delta) = & -m_\Phi^2 \Phi^\dagger \Phi + \frac{\lambda}{4} (\Phi^\dagger \Phi)^2 + M_\Delta^2 \text{Tr}(\Delta^\dagger \Delta) + [\mu (\Phi^T i \sigma^2 \Delta^\dagger \Phi) + \text{H.c}] \\ & + \lambda_1 (\Phi^\dagger \Phi) \text{Tr}(\Delta^\dagger \Delta) + \lambda_2 (\text{Tr} \Delta^\dagger \Delta)^2 + \lambda_3 \text{Tr}(\Delta^\dagger \Delta)^2 + \lambda_4 \Phi^\dagger \Delta \Delta^\dagger \Phi. \end{aligned} \quad (32)$$

Here, σ^2 is Pauli matrix. All Higgs self couplings λ_i ($i = \overline{1, 4}$) are considered as real parameters. For the EWSB, two Higgs multiplets are parameterized as follows:

$$\Delta = \frac{1}{\sqrt{2}} \begin{pmatrix} \delta^+ & \sqrt{2} \delta^{++} \\ v_\Delta + \eta_\Delta + i\chi_\Delta & -\delta^+ \end{pmatrix} \quad \text{and} \quad \Phi = \frac{1}{\sqrt{2}} \begin{pmatrix} \sqrt{2} \phi^+ \\ v_\Phi + \eta_\Phi + i\chi_\Phi \end{pmatrix}, \quad (33)$$

where vacuum expectation values (VEV) the two neutral Higgs are corresponding to v_Φ and v_Δ . The electroweak scale is fixed at $v = \sqrt{v_\Phi^2 + 2v_\Delta^2} \sim 246$ GeV for agreement with the SM case. In order to obtain the masses of physical scalar bosons, one rotates the flavor bases into the physics

states. The relations are shown as follows:

$$\begin{pmatrix} \phi^\pm \\ \delta^\pm \end{pmatrix} = \begin{pmatrix} c_{\beta^\pm} & -s_{\beta^\pm} \\ s_{\beta^\pm} & c_{\beta^\pm} \end{pmatrix} \begin{pmatrix} G^\pm \\ H^\pm \end{pmatrix}, \quad (34)$$

$$\begin{pmatrix} \eta_\Phi \\ \eta_\Delta \end{pmatrix} = \begin{pmatrix} c_\alpha & -s_\alpha \\ s_\alpha & c_\alpha \end{pmatrix} \begin{pmatrix} h^0 \\ H \end{pmatrix}, \quad (35)$$

and

$$\begin{pmatrix} \chi_\Phi \\ \chi_\Delta \end{pmatrix} = \begin{pmatrix} c_{\beta^0} & -s_{\beta^0} \\ s_{\beta^0} & c_{\beta^0} \end{pmatrix} \begin{pmatrix} G^0 \\ A^0 \end{pmatrix}, \quad (36)$$

where the rotation angles are given $t_{\beta^\pm} = \frac{\sqrt{2}v_\Delta}{v_\Phi}$, $t_{\beta^0} = \sqrt{2}t_{\beta^\pm}$ and the mixing angle α between two neutral Higgs is taken into account. After the EWSB, charged Nambu-Goldstone bosons G^\pm and neutral Nambu-Goldstone bosons G^0 are eaten by charged gauge bosons W^\pm and neutral gauge boson Z , respectively. As a result, all gauge bosons gain their masses. The remaining fields become the physical Higgs states. The Higgs spectrum of the THM includes pair of doubly charged Higgs $H^{\pm\pm}$, two singly charged H^\pm , a neutral CP-odd A^0 , and two CP-even H and h^0 being the SM-like Higgs boson. The masses of Higgses are expressed in terms of the Higgs self-coupling parameters and μ as follows:

$$M_{H^{\pm\pm}}^2 = \frac{\sqrt{2}\mu v_\Phi^2 - \lambda_4 v_\Phi^2 v_\Delta - 2\lambda_3 v_\Delta^3}{2v_\Delta}, \quad (37)$$

$$M_{H^\pm}^2 = \frac{(v_\Phi^2 + 2v_\Delta^2) [2\sqrt{2}\mu - \lambda_4 v_\Delta]}{4v_\Delta}, \quad (38)$$

$$M_{A^0}^2 = \frac{\mu(v_\Phi^2 + 4v_\Delta^2)}{\sqrt{2}v_\Delta}, \quad (39)$$

$$M_H^2 = \frac{1}{2} \left\{ \lambda v_\Phi^2 s_\alpha^2 + c_\alpha^2 \left[\sqrt{2}\mu \frac{v_\Phi^2}{v_\Delta} \left(1 + 4\frac{v_\Delta}{v_\Phi} t_\alpha \right) + 4v_\Delta^2 \left((\lambda_2 + \lambda_3) - (\lambda_1 + \lambda_4) \frac{v_\Phi}{v_\Delta} t_\alpha \right) \right] \right\}, \quad (40)$$

$$M_{h^0}^2 = \frac{1}{2} \left\{ \lambda v_\Phi^2 c_\alpha^2 + s_\alpha^2 \left[\sqrt{2}\mu \frac{v_\Phi^2}{v_\Delta} \left(1 - 4\frac{v_\Delta}{v_\Phi} t_\alpha \right) + 4v_\Delta^2 \left((\lambda_1 + \lambda_4) \frac{v_\Phi}{v_\Delta} t_\alpha + (\lambda_2 + \lambda_3) \right) \right] \right\}. \quad (41)$$

As same procedure, the Yukawa Lagrangian is expressed in terms of the mass eigenstates as follows:

$$\mathcal{L}_{\text{Yukawa}} = \mathcal{L}_{\text{Yukawa}}^{\text{SM}} - L_i^T y_\nu C(i\sigma^2 \Delta) L_i + \text{H.c.}, \quad (42)$$

where $L_i^T = (L_e, L_\mu, L_\tau)$ are three left-handed lepton doublets, y_ν is the 3×3 Yukawa coupling matrix and C is the charge conjugation operator. Expanding the Yukawa sector, one arrives the couplings of $A^0 \bar{f} f$ and $\phi \bar{f} f$ for $\phi = h_0, H$. The corresponding couplings are shown in Table 3. We also express the couplings in terms of κ -factors in the Table 3 as

$$g_{A^0 \bar{f} f} = -i\kappa_{A^0}^f \frac{m_f}{v} \gamma_5, \quad g_{\phi \bar{f} f} = -\kappa_\phi^f \frac{m_f}{v}. \quad (43)$$

Vertices	HESM	THM	κ -factors
$A^0 \bar{f} f$	$g_{A^0 \bar{\ell} \ell}$	$i \frac{\sqrt{2} t_{\beta^\pm}}{v} m_\ell \gamma_5$	$-\sqrt{2} t_{\beta^\pm}$
	$g_{A^0 \bar{d} d}$	$i \frac{\sqrt{2} t_{\beta^\pm}}{v} m_d \gamma_5$	$-\sqrt{2} t_{\beta^\pm}$
	$g_{A^0 \bar{u} u}$	$-i \frac{\sqrt{2} t_{\beta^\pm}}{v} m_u \gamma_5$	$\sqrt{2} t_{\beta^\pm}$
$\phi \bar{f} f$	$g_{h^0 \bar{f} f}$	$\frac{m_f}{v} c_\alpha$	$-c_\alpha$
	$g_{H \bar{f} f}$	$-\frac{v m_f}{v} s_\alpha$	s_α

Table 3: The couplings of $A^0 \bar{f} f$ and $\phi \bar{f} f$ are shown in this Table. We have used $\phi = h^0, H$ in the THM.

Other couplings relating to the processes under consideration are shown in Table 4. In this Table, the notations $V \equiv \gamma, Z$ and $\phi \equiv h^0, H$ are used.

Vertices	HESM	THM
$A^0 Z_\mu \phi$	$g_{A^0 Z h^0} \cdot (p_\mu^h - p_\mu^{A^0})$	$\frac{-ie}{s_{2W}} (2s_\alpha c_{\beta^0} - s_{\beta^0} c_\alpha) \cdot (p_\mu^h - p_\mu^{A^0})$
	$g_{A^0 Z H} \cdot (p_\mu^H - p_\mu^{A^0})$	$\frac{-ie}{s_{2W}} (2c_\alpha c_{\beta^0} + s_{\beta^0} s_\alpha) \cdot (p_\mu^H - p_\mu^{A^0})$
$\phi Z_\mu Z^\mu$	$-i \kappa_{h^0 ZZ} \cdot g_{h^0 ZZ}^{\text{SM}} \cdot g^{\mu\nu}$	$-i (c_{\beta^0} c_\alpha + 2s_\alpha s_{\beta^0}) \cdot g_{h^0 ZZ}^{\text{SM}} \cdot g^{\mu\nu}$
	$-i \kappa_{H ZZ} \cdot g_{h^0 ZZ}^{\text{SM}} \cdot g^{\mu\nu}$	$-i (-c_{\beta^0} s_\alpha + 2c_\alpha s_{\beta^0}) \cdot g_{h^0 ZZ}^{\text{SM}} \cdot g^{\mu\nu}$
$\phi W_\mu^\pm W_\nu^\mp$	$-i \kappa_{h^0 WW} \cdot g_{h^0 WW}^{\text{SM}} \cdot g^{\mu\nu}$	$-i (c_\alpha c_{\beta^\pm} + \sqrt{2} s_\alpha s_{\beta^\pm}) \cdot g_{h^0 WW}^{\text{SM}} \cdot g^{\mu\nu}$
	$-i \kappa_{H WW} \cdot g_{h^0 WW}^{\text{SM}} \cdot g^{\mu\nu}$	$-i (-s_\alpha c_{\beta^\pm} + \sqrt{2} c_\alpha s_{\beta^\pm}) \cdot g_{h^0 WW}^{\text{SM}} \cdot g^{\mu\nu}$

Table 4: All related couplings with $V \equiv \gamma, Z$ and $\phi \equiv h^0, H$ to the processes under consideration. Again, the couplings for SM-like Higgs vector boson pair in the SM are given $g_{h^0 ZZ}^{\text{SM}} = \frac{e M_W}{c_W^2 s_W}$, $g_{h^0 WW}^{\text{SM}} = \frac{e M_W}{s_W}$.

3. One-loop formulas for decay of $A^0 \rightarrow \ell \bar{\ell} V$ in HESM

In this section, the detailed evaluations for one-loop contributing the decay processes $A^0 \rightarrow \ell \bar{\ell} V$ in the HESM frameworks are presented. At tree-level, one has two following topologies contributing to the processes, as plotted in Fig. 1. When V becomes external photon, we have only the first topology relating to the decay channel. Noting that photon can attach to both lepton and anti-lepton. Therefore, we have two Feynman diagrams accordingly in this case. When V becomes Z boson, we have two additional diagrams showing in the second topology in Fig. 1. Here, ϕ can be the SM-like Higgs as well as other CP-even Higgses in the HESM.

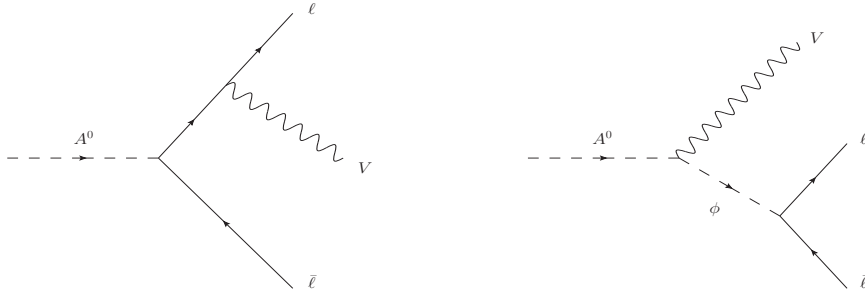


Figure 1: Tree-level topologies contributing to the decay processes. In the plots, $\phi = h^0$ for the SM-like Higgs boson and $\phi = H_j$ for remaining CP-even Higgses in the considered models.

Working in on-shell renormalization scheme, we have listed all topologies appear in the decay channels within 't Hooft-Feynman (HF) gauge at one-loop level. In all the below topologies, the first one-loop diagram in Fig. 2 (a) can be ignored, since there isn't the tree-level couplings of CP-odd Higgs to vector W , Z bosons. Within on-shell renormalization conditions, the counterterm diagram Fig. 2 (b) is included all field strength renormalizablized constants for external lines, the renormalizablized coupling constant for $A^0 f \bar{f}$, the renormalizablized mixing angle of A^0, G_0 , etc. However, this term is expressed in terms of tree-level amplitude and one-loop self-energies from the renormalizablized constants. Thus, the contribution is proportional to $y_\ell \times \mathcal{O}(\alpha)$ ($y_\ell = m_\ell/v$ is the Yukawa coupling). As a result, this contribution is assumed to be small in comparison with other ones and it can be omitted in the present paper, as same course of the works in Ref. [17, 18, 19, 66]. The next diagrams in Fig. 2 (c, d) as well as diagrams (e, f) in Fig. 3 also can be ignored in our current calculation because their contributions are proportional to $y_\ell \times \mathcal{O}(\alpha)$. Mixing of A^0 with ϕ (as plotted in diagram (g)) and mixing of ϕ with $V \equiv Z$ (depicted in diagram (h)) are vanished as shown in the appendices C, D. Self-energy diagrams in Fig. 4 (k, l) give zero contributions to the decay processes (see appendix D for detail). Furthermore, mixing of A^0 with $V \equiv Z, \gamma$ will be canceled due to Slavnov-Taylor identity [31].

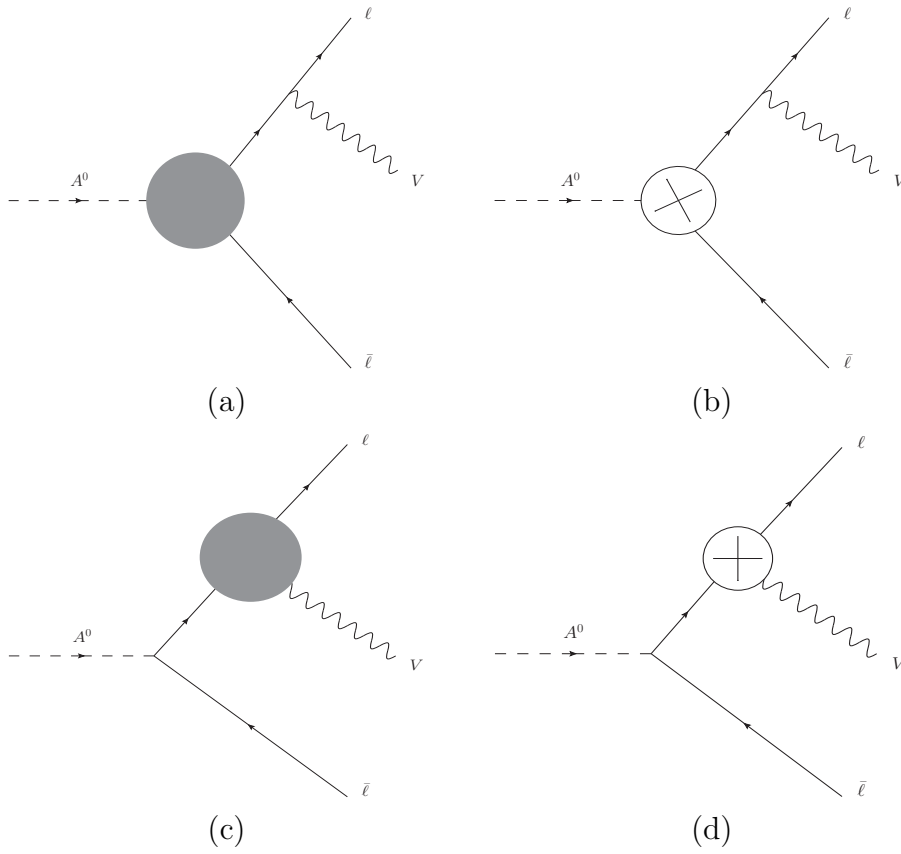


Figure 2: One-loop diagrams contributing to the decay processes $A^0 \rightarrow \ell \bar{\ell} V$ in HESM within the HF gauge.

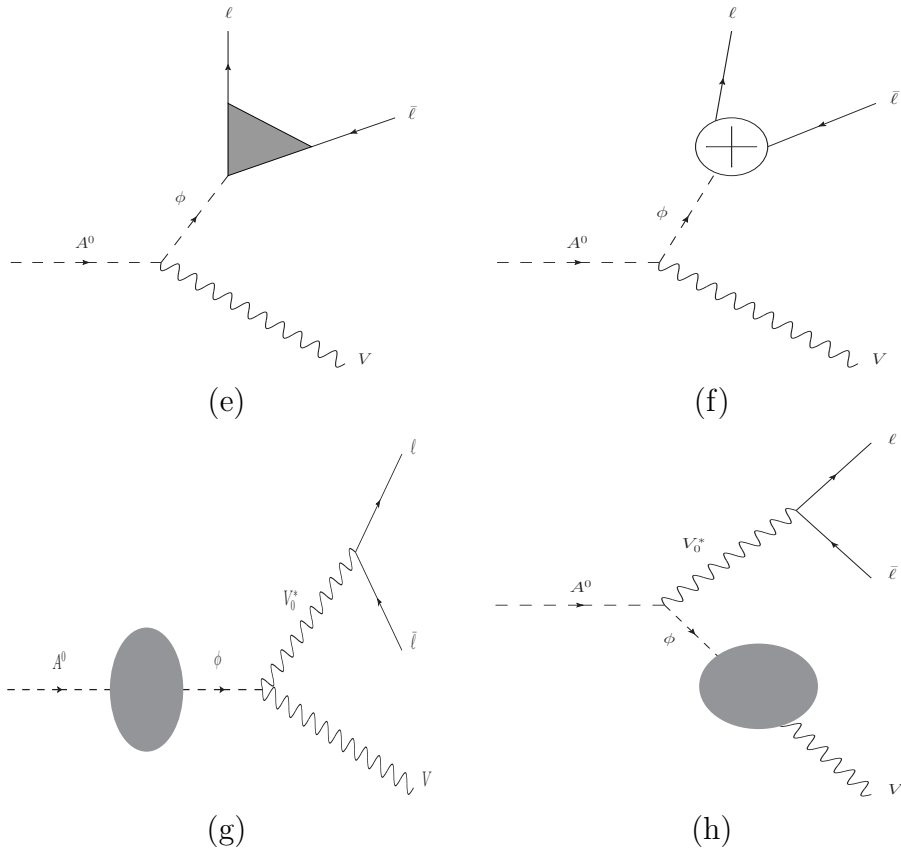


Figure 3: One-loop diagrams contributing to the decay processes $A^0 \rightarrow \ell \bar{\ell} V$ in HESM within the HF gauge.

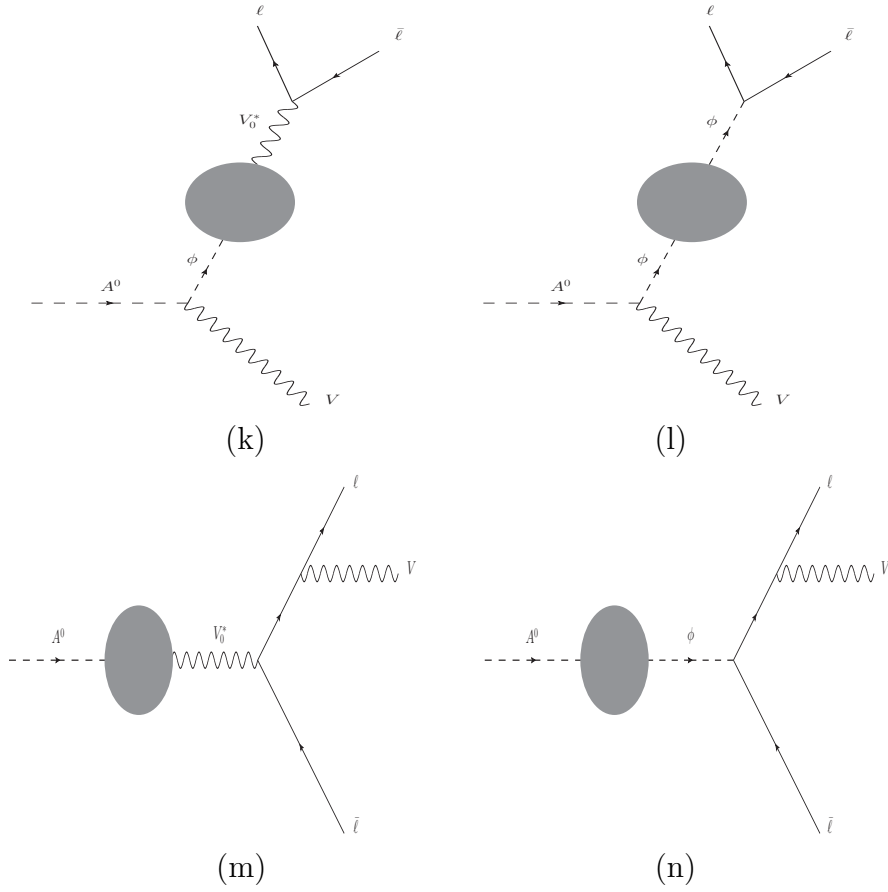


Figure 4: One-loop diagrams contributing to the decay processes $A^0 \rightarrow \ell\bar{\ell}V$ in HESM within the HF gauge.

Lastly, we list all Feynman diagrams contributing to the processes under consideration in Fig. 5. They are considered to be dominant contributions to the processes. In the first topology (o), CP-odd Higgs only couple to fermions, we hence have fermion loop in this case. The dominant contributions are from top, bottom quarks and tau lepton exchanging in the loop. The diagram (p), one takes into account W, Z propagating in the loop. Finally, we have box diagram (q) with Z boson exchanging in the loop contributing to the processes.

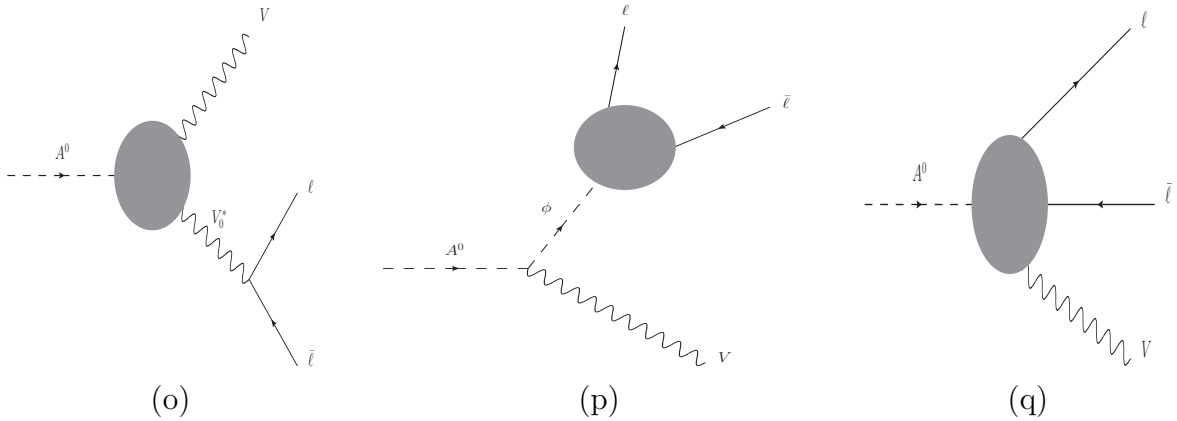


Figure 5: One-loop diagrams contributing to the decay processes $A^0 \rightarrow \ell\bar{\ell}V$ in HESM within the HF gauge. They are considered to be dominant contributions to the processes.

The total amplitude for the decay $A^0(p) \rightarrow \ell(q_1)\bar{\ell}(q_2)V_\mu(q_3)$ is expressed as the sum of each group G_i for $i = 1, 2, 3$ listed in the following paragraphs

$$\mathcal{A}_{\text{Total}} = \mathcal{A}_{\text{Tree}}^{A^0 \rightarrow \ell\bar{\ell}V} + \mathcal{A}_{\text{1-loop}}^{A^0 \rightarrow \ell\bar{\ell}V}. \quad (44)$$

The related kinematic variables for the processes are included as follows:

$$p^2 = M_{A^0}^2, \quad q_1^2 = q_2^2 = m_\ell^2, \quad q_3^2 = M_V^2, \quad q_{jk} = (q_j + q_k)^2 \quad \text{for } j, k = 1, 2, 3. \quad (45)$$

The above kinematic variables follow the relation:

$$q_{12} + q_{13} + q_{23} = M_{A^0}^2 + M_V^2 + 2m_\ell^2 \simeq M_{A^0}^2 + M_V^2. \quad (46)$$

First, tree-level amplitude for the decay processes $A^0 \rightarrow \ell\bar{\ell}V$ can be expressed as follows:

$$\begin{aligned} \mathcal{A}_{\text{tree}}^{A^0 \rightarrow \ell\bar{\ell}V} &= \frac{i\kappa_{A^0}^\ell}{(q_{13} - m_\ell^2)(q_{23} - m_\ell^2)} \cdot \frac{m_\ell}{v} \cdot u(q_1) \left\{ 2(q_{13} - m_\ell^2) \left(\mathbf{a}_{V\ell\bar{\ell}} - \mathbf{v}_{V\ell\bar{\ell}} \gamma_5 \right) p \cdot \epsilon^*(q_3) \right. \\ &\quad \left. + \left[\mathbf{a}_{V\ell\bar{\ell}} (q_{23} - q_{13}) + \mathbf{v}_{V\ell\bar{\ell}} (q_{13} + q_{23} - 2m_\ell^2) \gamma_5 \right] \not{p} \not{\epsilon}^*(q_3) \right\} \bar{v}(q_2) \\ &\quad + \sum_{\phi=h^0, H_j} i \frac{2m_\ell}{q_{12} - M_\phi^2} g_{\phi A^0 V} \left\{ u(q_1) \left[\mathbf{v}_{\phi\ell\bar{\ell}} + \mathbf{a}_{\phi\ell\bar{\ell}} \gamma_5 \right] \bar{v}(q_2) \right\} p \cdot \epsilon^*(q_3). \end{aligned} \quad (47)$$

For CP-even Higgs boson $\phi \equiv h^0, H_j$, the axial-vector components $\mathbf{a}_{\phi\ell\bar{\ell}} = 0$ for the CP-conserving case. In the above formulas, when V or V_0^* being Z -boson, one has $M_V^2 = M_Z^2$, $\Gamma_{V_0} = \Gamma_Z$ and the involved couplings are replaced by

$$\mathbf{v}_{Zf\bar{f}} = \frac{e}{s_{2W}} (I_{3,f} - 2s_W^2 Q_f), \quad \mathbf{a}_{Zf\bar{f}} = -\frac{e}{s_{2W}} I_{3,f}. \quad (48)$$

In the case of V or V_0^* being photon, one has $M_V^2 = 0$, $\Gamma_{V_0} = 0$ and the corresponding couplings read as

$$\mathbf{v}_{\gamma f\bar{f}} = eQ_f, \quad \mathbf{a}_{\gamma f\bar{f}} = 0. \quad (49)$$

We next consider one-loop amplitude which can be evaluated from Fig. 5. These diagrams are divided into three following groups in Figs. 6, 7, 8. In detail, one-loop amplitude is calculated as follows:

$$\mathcal{A}_{\text{1-loop}} = \sum_{i=1}^3 \mathcal{A}_{G_i}^V. \quad (50)$$

Where V can be external photon γ and Z boson. Each one-loop amplitude can be derived in the following paragraphs. It is noted that V being γ , we have only one diagram in Fig. 6 attributing to the amplitude. When V become external Z boson, we take into account two more topologies in Figs. 7, 8 contributing to the amplitude.

We first arrive at group G_1 (as depicted in Fig. 6) in which one-loop Feynman triangle diagrams with V_0^* -pole. We denote that V_0^* can be γ^*, Z^* in this calculation. Since, there is no the coupling of CP-odd Higgs with vector boson at tree-level. We have only fermion loop in this case.

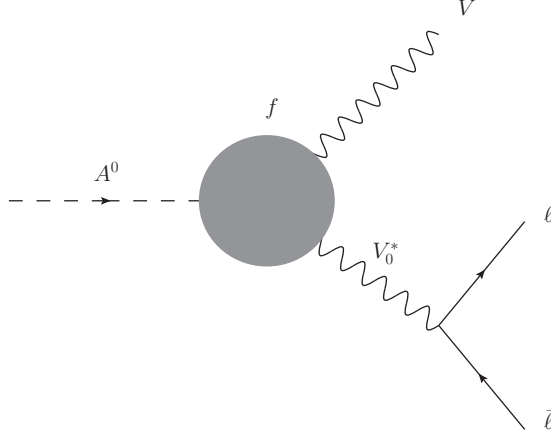


Figure 6: Group 1–One-loop Feynman diagrams V_0^* -poles contributing to the processes. We denote that V_0^* can be γ^*, Z^* in this calculation.

Considering all fermions f exchanging in loop, one-loop amplitude reads as follows:

$$\mathcal{A}_{G_1}^{(V)} = \sum_{V_0^*=\gamma^*, Z^*} \sum_f u(q_1) \left[(\mathbf{v}_{V_0^* \ell \bar{\ell}} - \mathbf{a}_{V_0^* \ell \bar{\ell}} \gamma_5) \gamma^\mu \right] \bar{v}(q_2) \frac{F_{G_1, f}^{(V)} \cdot (\varepsilon_{\mu\nu\rho\sigma} p^\rho q_3^\sigma) \cdot \epsilon^{*\nu}(q_3)}{(q_{12} - M_{V_0}^2) + iM_{V_0} \Gamma_{V_0}}. \quad (51)$$

In this formulas, $\varepsilon_{\mu\nu\rho\sigma}$ anti-symmetry tensor Levi-civita is taken into account. While one-loop form factor $F_{G_1, f}^{(V)}$ is written in terms of scalar one-loop integrals in the form of

$$\begin{aligned} F_{G_1, f}^{(V)} &= i \frac{\kappa_{A_0}^f}{2\pi^2} \frac{N_f^C m_f^2}{[M_{A_0}^4 - 2M_{A_0}^2(M_V^2 + q_{12}) + (M_V^2 - q_{12})^2]} \cdot \frac{m_f}{v} \times \\ &\times \left\{ 2 \mathbf{a}_{V_0^* f \bar{f}} \mathbf{a}_{V f \bar{f}} \left[(q_{12} - M_{A_0}^2 - M_V^2) B_0(M_V^2, m_f^2, m_f^2) \right. \right. \\ &\quad \left. \left. + (M_V^2 - M_{A_0}^2 - q_{12}) B_0(q_{12}, m_f^2, m_f^2) + 2M_{A_0}^2 B_0(M_{A_0}^2, m_f^2, m_f^2) \right] \right. \\ &\quad \left. + \left[\mathbf{v}_{V_0^* f \bar{f}} \mathbf{v}_{V f \bar{f}} \left(2M_{A_0}^2 (M_V^2 + q_{12}) - (M_V^2 - q_{12})^2 - M_{A_0}^4 \right) \right. \right. \\ &\quad \left. \left. + \mathbf{a}_{V_0^* f \bar{f}} \mathbf{a}_{V f \bar{f}} \left(M_{A_0}^4 - (M_V^2 - q_{12})^2 \right) \right] C_0(M_V^2, q_{12}, M_{A_0}^2, m_f^2, m_f^2, m_f^2) \right\}. \end{aligned} \quad (52)$$

We next consider one-loop amplitudes with ϕ -poles including the W^\pm bosons and Z boson exchanging in the loop (seen Fig. 7). In this case, we note ϕ for h^0 or new heavy CP-even Higgses H_j in the considered models. Evaluating the processes in THDM and THM, we have $H_j = H$.

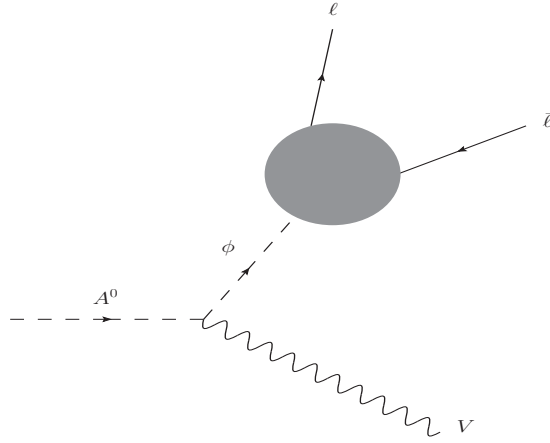


Figure 7: Group 2– One-loop Feynman diagrams with ϕ -poles including the W^\pm bosons and Z boson exchanging in the loop.

The amplitude is decomposed in form of

$$\mathcal{A}_{G_2}^V = \sum_{\phi=h^0, H_j} \left[u(q_1) \mathbf{1} \bar{v}(q_2) \right] \times \left[\sum_{P=W/Z} F_{G_2, P}^{(V)} \right] \times \frac{[p \cdot \epsilon^*(q_3)]}{(q_{12} - M_\phi^2)}. \quad (53)$$

One-loop form factors are expressed as follows

$$F_{G_2, W}^{(V)} = -\frac{i \alpha}{2\pi s_W^2} \frac{m_\ell}{q_{12} - 4m_\ell^2} \cdot g_{\phi A^0 V} \cdot g_{\phi W W} \times \quad (54)$$

$$\times \left[B_0(m_\ell^2, 0, M_W^2) - B_0(q_{12}, M_W^2, M_W^2) + (M_W^2 - m_\ell^2) C_0(m_\ell^2, q_{12}, m_\ell^2, 0, M_W^2, M_W^2) \right],$$

$$F_{G_2, Z}^{(V)} = -\frac{i}{2\pi^2} \frac{m_\ell}{q_{12} - 4m_\ell^2} \cdot g_{\phi A^0 V} \cdot g_{\phi Z Z} \times \quad (55)$$

$$\times \left\{ \left[(\mathbf{a}_{Z\ell\bar{\ell}})^2 + (\mathbf{v}_{Z\ell\bar{\ell}})^2 \right] \left[B_0(m_\ell^2, m_\ell^2, M_Z^2) - B_0(q_{12}, M_Z^2, M_Z^2) \right] \right.$$

$$\left. + \left[(\mathbf{a}_{Z\ell\bar{\ell}})^2 (M_Z^2 + q_{12} - 6m_\ell^2) + (\mathbf{v}_{Z\ell\bar{\ell}})^2 (M_Z^2 - q_{12} + 2m_\ell^2) \right] C_0(m_\ell^2, q_{12}, m_\ell^2, m_\ell^2, M_Z^2, M_Z^2) \right\}.$$

Finally, we concern the group G_3 (as Fig. 8), taking all one-loop Feynman box diagrams which have $\phi \equiv h^0, H_j$ with H_j being new heavy CP-even Higgses in the mentioned models and $V \equiv Z$ boson propagating in the loop.

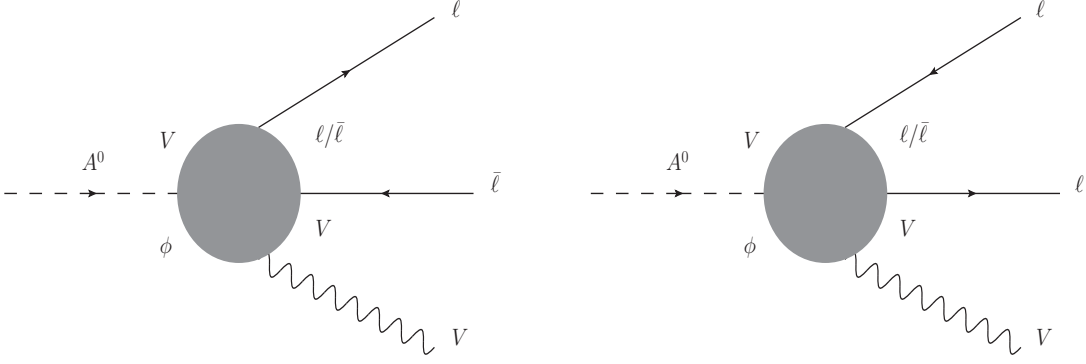


Figure 8: Group 3– One-loop box diagrams with exchanging Z boson and ϕ in the loop.

The corresponding one-loop amplitude can be written in the form of

$$\mathcal{A}_{G_3}^V = \sum_{\phi=h^0, H_j} u(q_1) \left\{ (\mathbf{a}_{Z\ell\bar{\ell}})^2 + (\mathbf{v}_{Z\ell\bar{\ell}})^2 - 2 \mathbf{a}_{Z\ell\bar{\ell}} \mathbf{v}_{Z\ell\bar{\ell}} \gamma_5 \right\} \times \left\{ F_{0,G_3}^{(V)} \times \not{\epsilon}^*(q_3) + \sum_{k=1,2} F_{k,G_3}^{(V)} \cdot [q_k \cdot \epsilon^*(q_3)] \times \not{p} \right\} \bar{v}(q_2). \quad (56)$$

The one-loop form factors are expressed in terms of scalar one-loop functions as follows:

$$F_{0,G_3}^{(V)} = -\frac{i g_{\phi A^0 Z} \cdot g_{\phi Z V}}{16\pi^2} \left\{ C_0(m_\ell^2, M_V^2, q_{13}, m_\ell^2, M_Z^2, M_\phi^2) + M_Z^2 D_0(m_\ell^2, q_{12}, M_V^2, q_{13}, m_\ell^2, M_{A^0}^2, m_\ell^2, M_Z^2, M_Z^2, M_\phi^2) + 2[q_{13} - M_{A^0}^2] D_1(m_\ell^2, q_{12}, M_V^2, q_{13}, m_\ell^2, M_{A^0}^2, m_\ell^2, M_Z^2, M_Z^2, M_\phi^2) + q_{12} D_2(m_\ell^2, q_{12}, M_V^2, q_{13}, m_\ell^2, M_{A^0}^2, m_\ell^2, M_Z^2, M_Z^2, M_\phi^2) + [q_{13} + M_{A^0}^2] D_3(m_\ell^2, q_{12}, M_V^2, q_{13}, m_\ell^2, M_{A^0}^2, m_\ell^2, M_Z^2, M_Z^2, M_\phi^2) \right\} \quad (57)$$

$$F_{1,G_3}^{(V)} = -\frac{i g_{\phi A^0 Z} \cdot g_{\phi Z V}}{4\pi^2} D_2(m_\ell^2, q_{12}, M_V^2, q_{13}, m_\ell^2, M_{A^0}^2, m_\ell^2, M_Z^2, M_Z^2, M_\phi^2), \quad (58)$$

$$F_{2,G_3}^{(V)} = -F_{1,G_3}^{(V)} \left\{ q_{13} \leftrightarrow q_{23} \right\}. \quad (59)$$

After collecting the one-loop form factors, we check numerically for the calculation by verifying all factors are ultraviolet (UV) and infrared (IR) finiteness. One finds the results are good stability. In this paper, we skip showing numerical results of the test. Since the information is not important for our discussion (see our previous works for example of the numerical test [17, 19, 66]). Having all correctness one-loop amplitudes, the decay rates are then evaluated as follows:

$$\Gamma_{A^0 \rightarrow \ell\bar{\ell}V} = \frac{1}{256\pi^3 M_{A^0}^3} \int_{q_{12}^{\min}}^{q_{12}^{\max}} dq_{12} \int_{q_{13}^{\min}}^{q_{13}^{\max}} dq_{13} \sum_{\text{pol.}} |\mathcal{A}_{\text{Total}}|^2. \quad (60)$$

Where the total amplitude is expressed as follows:

$$\sum_{\text{pol.}} |\mathcal{A}_{\text{Total}}|^2 = \sum_{\text{pol.}} |\mathcal{A}_{\text{Tree}}|^2 + 2 \sum_{\text{pol.}} \mathcal{R}e \left\{ \mathcal{A}_{\text{Tree}}^* \mathcal{A}_{\text{Loop}} \right\} + \sum_{\text{pol.}} |\mathcal{A}_{\text{Loop}}|^2. \quad (61)$$

The limitations of integration are expressed for the general vector boson V in final state as follows:

$$q_{12}^{\min} = 4m_\ell^2, \quad (62)$$

$$q_{12}^{\max} = (M_{A^0} - M_V)^2, \quad (63)$$

$$q_{13}^{\max(\min)} = \frac{M_{A^0}^2 + M_V^2 + 2m_\ell^2 - q_{12}}{2} \pm \frac{1}{2} \sqrt{\left(1 - \frac{4m_\ell^2}{q_{12}}\right) \left[(M_{A^0}^2 + M_V^2 - q_{12})^2 - 4M_{A^0}^2 M_V^2 \right]}. \quad (64)$$

We comment that the last term in Eq. (61) belong to order of two-loop corrections. However, as we show in later since the interference between tree and one-loop amplitude to be very small contributions. This behavior also holds for the interference between tree and two-loop amplitude. With light fermions in final states in scalar particle decays, the loop amplitude is dominant contributions as many previous works [18, 17, 19, 66]. Therefore, we also take the last term in Eq. (61) into account for our analysis.

4. Phenomenological results

In the phenomenological results, we focus on two typical HESMs in this paper such as THDM and THM as examples. For numerical results in this work, we apply the input parameters as follows. For the masses of gauge bosons and their decay widths, one takes $M_Z = 91.1876$ GeV, $\Gamma_Z = 2.4952$ GeV, $M_W = 80.379$ GeV, $\Gamma_W = 2.085$ GeV. The mass of the SM-like Higgs boson and its total decay width are $M_{h^0} = 125.1$ GeV, $\Gamma_{h^0} = 4.07 \cdot 10^{-3}$ GeV. For fermion sector, we use the input parameters as $m_e = 0.00052$ GeV, $m_\mu = 0.10566$ GeV and $m_\tau = 1.77686$ GeV. In the quark sector, their masses are taken as $m_u = 0.00216$ GeV, $m_d = 0.0048$ GeV, $m_c = 1.27$ GeV, $m_s = 0.93$ GeV, $m_t = 173.0$ GeV, and $m_b = 4.18$ GeV. The G_μ -scheme is taken into account for the following numerical investigations. In this scheme, the Fermi constant is treated as an input parameter with the value $G_\mu = 1.16638 \cdot 10^{-5}$ GeV⁻². The electroweak constant is then obtained subsequently:

$$\alpha = \sqrt{2}/\pi G_\mu M_W^2 (1 - M_W^2/M_Z^2) = 1/132.184. \quad (65)$$

We note that the other input parameters for generating the decay rate and its distributions are scanned appropriately in the parameter space corresponding to the models under consideration.

4.1. THDM

We first arrive at the phenomenological analysis for THDM. In detail, we are going to examine the decay rates of CP-odd Higgs decay into $\ell\bar{\ell}V$ with V being photon and Z boson. Besides that, we also interested in the differential decay widths with respect to the invariant mass of lepton pair. Before studying the detailed physical results, we first review briefly the current parameter space for THDM, e.g. the theoretical and experimental constraints on physical parameter space for THDM. It is well-known that theoretical constraints reply on tree-level unitarity of the theory, vacuum stability conditions for the scalar Higgs potential as well as the requirements of perturbative regime. These subjects have examined in Refs. [40, 41, 42, 43, 45]. Following the above

constraints, the theoretical bounds on the parameters λ_i for $i = 1, 2, \dots, 5$ and m_{11}, m_{12}, m_{22} have given in the above references. In the aspect of the experimental limitations, the electroweak precision tests (EWPT) for THDM have implicated at LEP [46, 47]. Furthermore, from the direct and indirect searching for the masses of scalar particles in THDM have performed at the LEP, the Tevaron and the LHC as summarized in [44]. In addition, implicating for one-loop induced decays of $h \rightarrow \gamma\gamma$ and $h \rightarrow Z\gamma$ in THDM have performed in Refs. [20, 21] and the references therein. Combining all the above constraints, we can take logically the parameter space for our analysis in THDM as follows. We select $126 \text{ GeV} \leq M_H \leq 1000 \text{ GeV}$, $60 \text{ GeV} \leq M_{A^0} \leq 1000 \text{ GeV}$ and $80 \text{ GeV} \leq M_{H^\pm} \leq 1000 \text{ GeV}$ in the type I and type X of THDM. For the Type-II and Y, we can scan consistently the physical parameters as follows: $500 \text{ GeV} \leq M_H \leq 1000 \text{ GeV}$, $500 \text{ GeV} \leq M_{A^0} \leq 1000 \text{ GeV}$ and $580 \text{ GeV} \leq M_{H^\pm} \leq 1500 \text{ GeV}$. In both types, one takes $2 \leq t_\beta \leq 20$, $0.95 \leq s_{\beta-\alpha} \leq 1$ for the alignment limit of the SM (we take $s_{\beta-\alpha} = 0.995$ for all below physical results) and $m_{12}^2 = M_H^2 s_\beta c_\beta$. Furthermore, the constraints on t_β , M_{H^\pm} from flavor experimental data have also performed for the THDM with the softly broken Z_2 symmetry in Ref. [65]. In Ref. [65], the small values of t_β are favoured in explaining the flavor experimental data. To complete our discussions, we are also interested in considering the small values of t_β (scan it reasonably over the region of $2 \leq t_\beta \leq 10$ for examples) in our work. In our analysis, the decay widths of SM-like Higgs is taken from experimental value. While the total decay width of CP-even Higgs H is calculated at LO as in [14] (see Appendix B for more detail). We are going to present the phenomenological results for all decay processes $A^0 \rightarrow \ell\bar{\ell}\gamma, \ell\bar{\ell}Z$ in THDM in the following subsections. We emphasize that we only study phenomenological results for THDM with types I, II because there are same Yukawa couplings in types I and X as well as types II and Y.

4.1.1. Decay processes $A^0 \rightarrow \ell\bar{\ell}\gamma$

First, the physical results for decay channels $A^0 \rightarrow \ell\bar{\ell}\gamma$ in THDM are presented. The effects of one-loop contributing to the decay rates are examined. The total decay widths as a function of M_{A^0} at $t_\beta = 5, 10$ are shown in Fig. 15. In the plots, we change $150 \text{ GeV} \leq M_{A^0} \leq 600 \text{ GeV}$. In the left panel figures, the physical results for the THDM with type I are shown at $t_\beta = 5$ (in the above figure) and $t_\beta = 10$ (in the below figure), respectively. While the similar data for the THDM with type II is plotted in the right panel figures. In the plots, the black-dotted points are for total decay rates and the red-squared points show for tree-level decay widths. While the triangle points with green color present for one-loop the decay widths and the blue-squared points are the decay rates calculated from the interference between tree and one-loop amplitudes. It is interested to observe that the one-loop decay widths are dominant in this case. In general, the decay rates are proportional to M_{A^0} and $1/t_\beta$. In all scatter plots, the small figures in the corner of each plot show for the decay widths computing from the absolute value of the interference between tree and one-loop amplitudes. It is indicated that these terms give a very small contributions in comparison with other ones. As a result, the contributions can be omitted as we discussed in previous section. From the data, the one-loop effects on the decay rates are significance attributions and they should be taken into account for physical analysis.

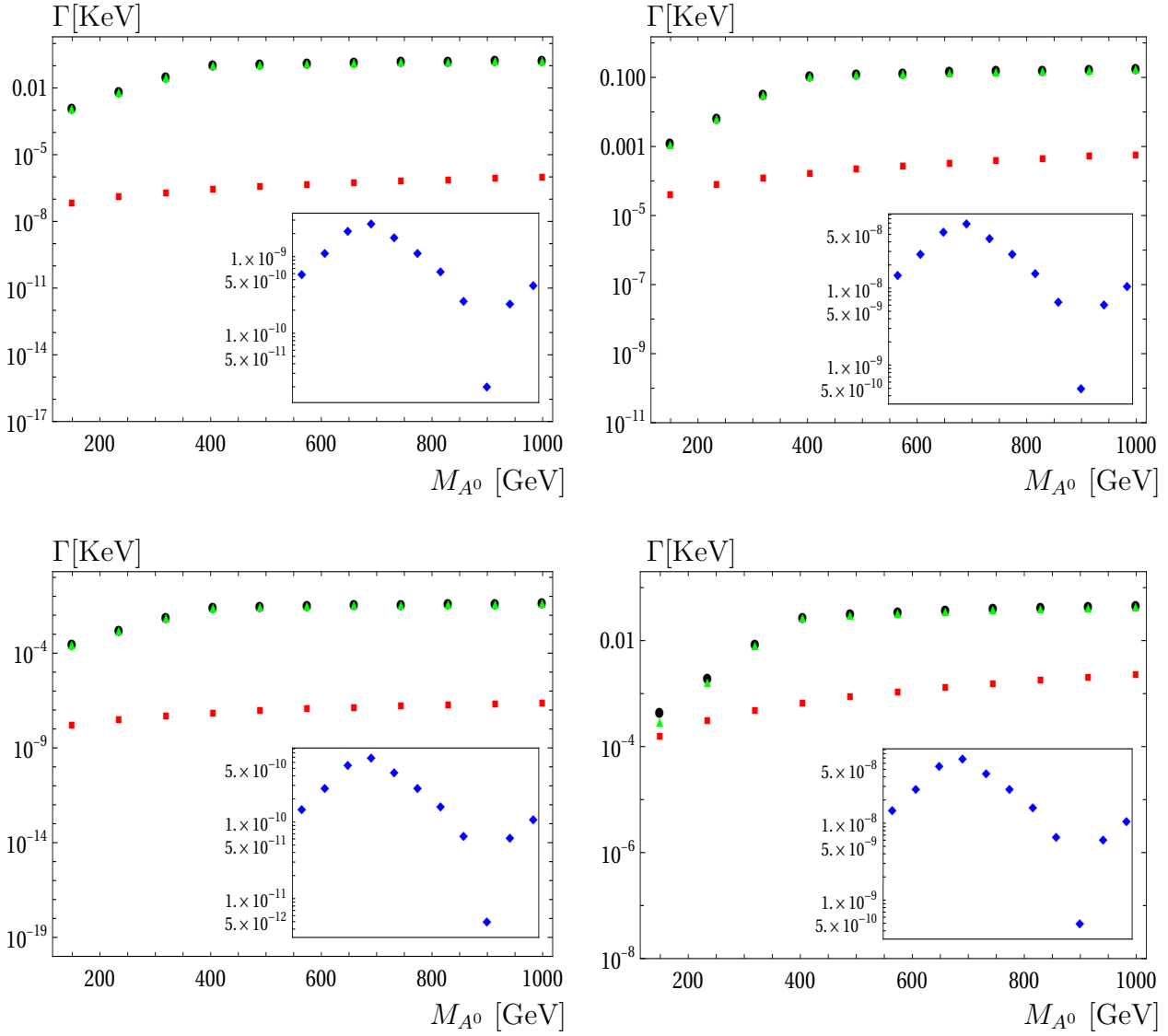


Figure 9: Total decay rates for $A^0 \rightarrow \ell\bar{\ell}\gamma$ in the THDM with types I and II are presented. In the left panel, we show the decay rates at $t_\beta = 5$ (the above figure) and at 10 (the below figure) for the THDM with type I. We present the decay rates at $t_\beta = 5, 10$ for the THDM with type II in the right panel, as same convention. In the plots, we vary $150 \text{ GeV} \leq M_{A^0} \leq 1000 \text{ GeV}$.

Differential decay rates with respect to $m_{\ell\ell}$ for $A^0 \rightarrow \ell\bar{\ell}\gamma$ as function of t_β in the THDM with types I and II are shown in Fig. 10 for type I (on the left panel) and for type II (on the right panel). In the plots, we set $M_{A^0} = 200 \text{ GeV}$ for all the above figures and $M_{A^0} = 500 \text{ GeV}$ for all the below figures, respectively. In the plots, we vary $2 \leq t_\beta \leq 10$. Overall, we find that the decay rates are decreased with $m_{\ell\ell}$. There are two peaks observing in the differential decay widths which are corresponding to γ^* -peak and Z^* -peak. The decay rates develop to the peaks and are decrease rapidly with $m_{\ell\ell}$ beyond the peaks. Moreover, expression for one-loop form factors in Eq. (52) indicates that the form factors are largest at $q_{12} = m_{\ell\ell}^2 \rightarrow M_{A^0}^2$. In fact, the one-loop factors in Eq. (52) are taken the form of

$$F_{G_{1,f}}^{(\gamma)} \sim \frac{1}{[M_{A^0}^4 - 2M_{A^0}^2(M_V^2 + q_{12}) + (M_V^2 - q_{12})^2]|_{M_V^2=0}} = \frac{1}{[q_{12} - M_{A^0}^2]^2}. \quad (66)$$

Subsequently, one finds the peak of decay rates at $m_{\ell\ell} \rightarrow M_{A^0}$. The data is also shown that the decay rates are inversely proportional to t_β . At tree-level amplitude in THDM with type II,

we find that the couplings of A^0 to lepton pair are proportional to t_β as in Table 1. At high mass region of M_{A^0} , the decay rates of tree level amplitude are more significance contributions, as indicated in previous data. It explains for the reason that decay rates are proportional to t_β in high mass regions of M_{A^0} in THDM with type II.

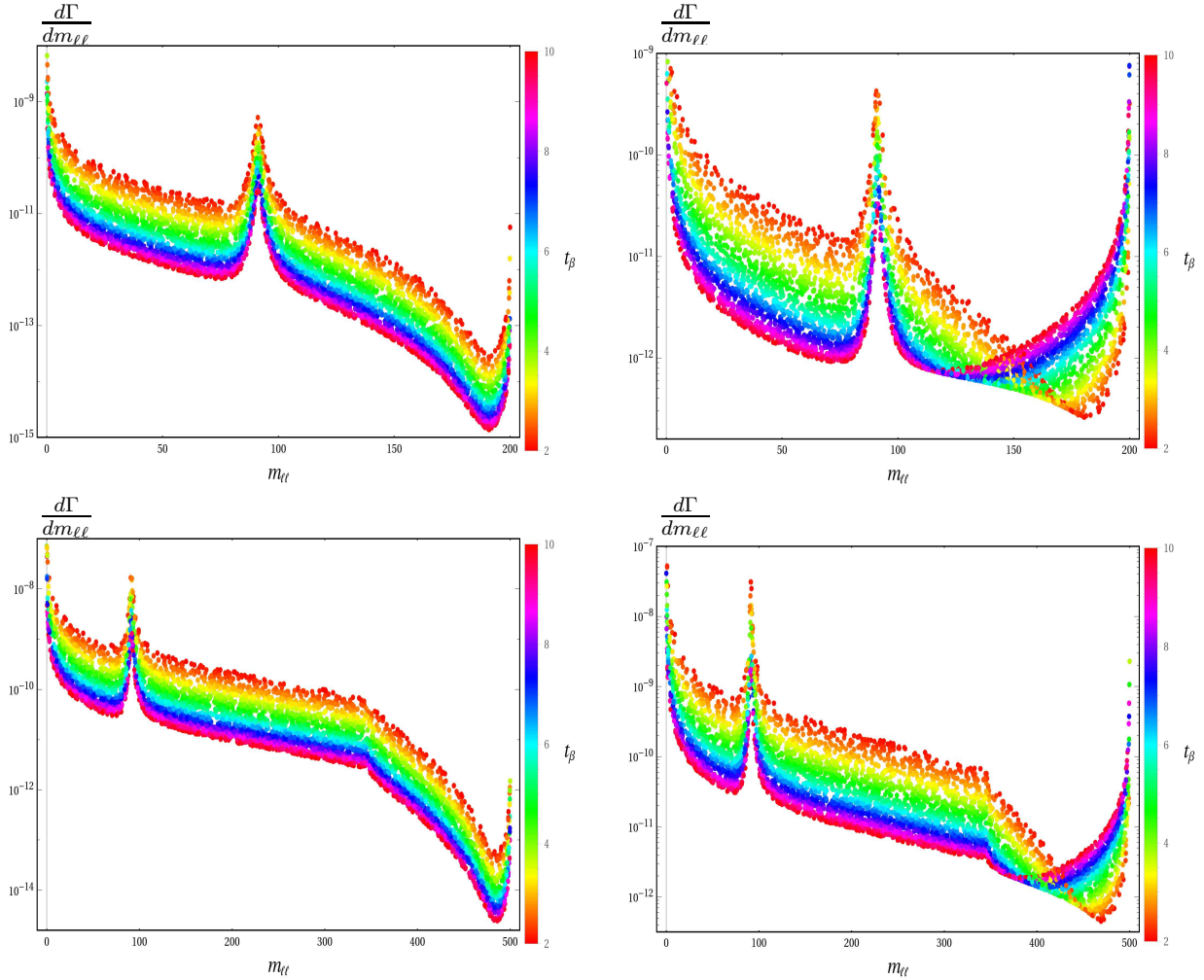


Figure 10: Differential decay rates with respect to $m_{\ell\ell}$ for $A^0 \rightarrow \ell\bar{\ell}\gamma$ as function of t_β in the THDM with types I and II. In the left panel, we show the decay rates at $M_{A^0} = 200$ (above figure) and at 500 GeV (below figure) for the THDM with type I. We present the decay rates at $M_{A^0} = 200, 500$ GeV for the THDM with type II in the right panel, as same convention. In the plots, we vary $2 \leq t_\beta \leq 10$.

4.1.2. Decay processes $A^0 \rightarrow \ell\bar{\ell}Z$

We turn our attention to the decay processes $A^0 \rightarrow \ell\bar{\ell}Z$. In Fig. 11, we present the total decay rates of $A^0 \rightarrow \ell\bar{\ell}Z$ as functions of M_{A^0} at $t_\beta = 5, 10$ for both types I and II of THDM. The data points are presented in these plots following the same previous notations. In all plots, we set $300 \text{ GeV} \leq M_{A^0} \leq 1000 \text{ GeV}$. We show the results for type I of THDM on the left panel of the figures at $t_\beta = 5$ (the above plot) and $t_\beta = 10$ (the below plot). The same data for type II of THDM is shown in the right panel. In all plots, the small figures in the right corner of each figure, we plot the decay rates of the interference between tree amplitude and one-loop amplitude. Again, there contributions are much smaller than other contributions and can be ignored in this calculation. To avoid the numerical instability of the results which are from the narrow peak of SM-like Higgs boson, one applies a cut on $q_{12} \geq q_{12}^{\min} = (M_{h^0}^2 + 1) \text{ GeV}^2$.

Generally, one find that the decay rates are proportional to M_{A_0} . Difference from the channels $A^0 \rightarrow \ell\bar{\ell}\gamma$, in processes $A^0 \rightarrow \ell\bar{\ell}Z$, we don't find that the decay rates depend certainly on t_β in type I and are proportional to t_β in type II. We observe that one-loop contributing for the decay rates are significance and they should be taken into account for physical analysis.

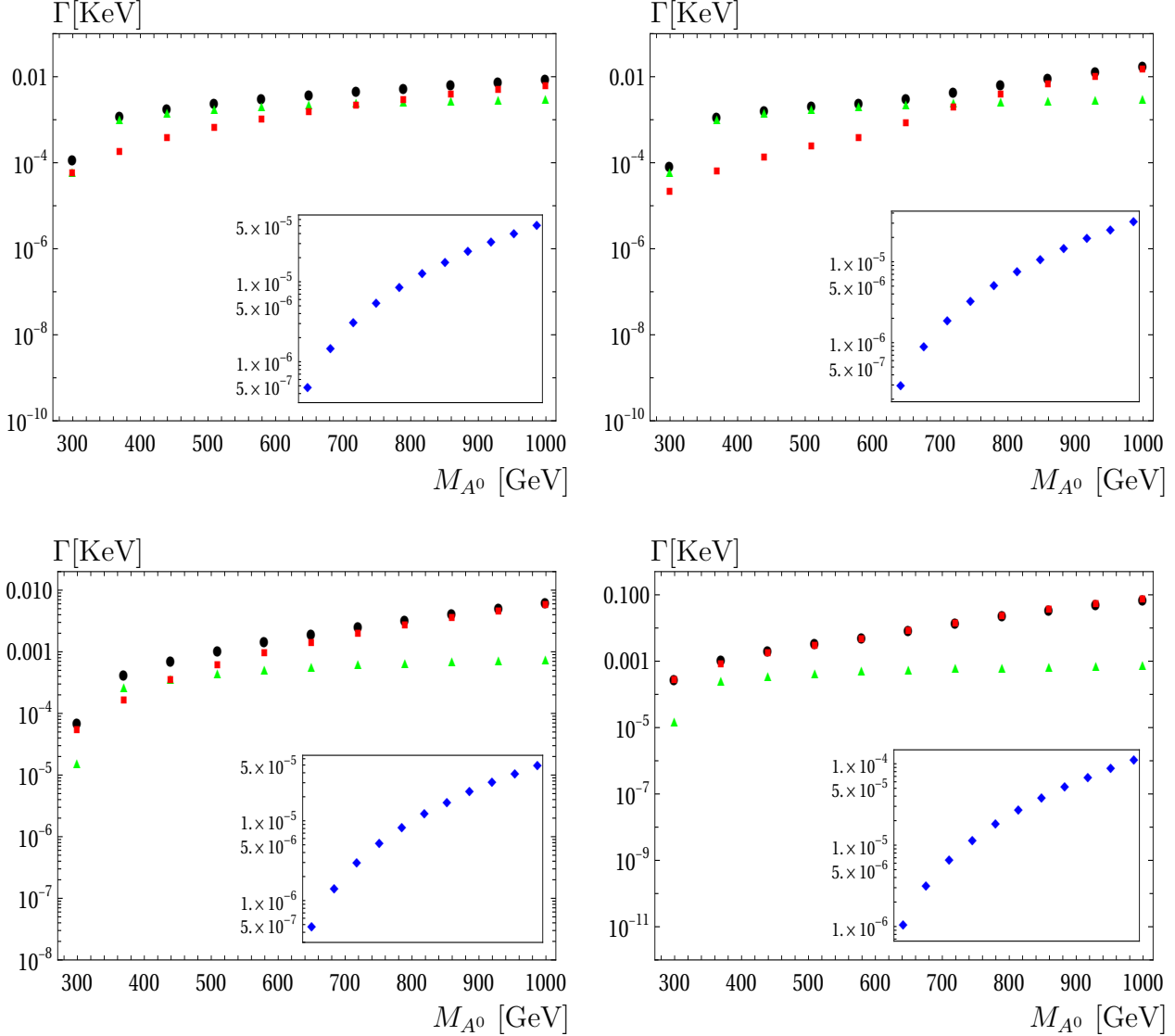


Figure 11: Total decay rates for $A^0 \rightarrow \ell\bar{\ell}Z$ in the THDM with types I and II are shown in the plots. In the left panel, we show the decay rates at $t_\beta = 5$ (above figure) and at 10 (below figure) for the THDM with type I. We present the decay rates at $t_\beta = 5, 10$ for the THDM with type II in the right panel as same notation. In the plots, we vary $300 \text{ GeV} \leq M_{A^0} \leq 1000 \text{ GeV}$ and take $M_H = 500 \text{ GeV}$. To avoid the numerical instability of the results, one applies a cut on $q_{12} \geq q_{12}^{\min} = (M_{h^0}^2 + 1) \text{ GeV}^2$.

We also interested in the differential decay rates with respect to $m_{\ell\ell}$ as shown in Fig. 12. In the processes $A^0 \rightarrow \ell\bar{\ell}Z$ we have two more one-loop topologies (Figs. 7, 8) contributing to the channels. In the left panel figures, the results for THDM with type I are shown at $M_{A_0} = 300 \text{ GeV}$ (in above figure) and at $M_{A_0} = 800 \text{ GeV}$ (in below figure). The corresponding results for THDM with type II are presented in right panel plots. In general, we observe the same behave of the decay rates in the case of $A^0 \rightarrow \ell\bar{\ell}\gamma$, or the decay rates are generally decreased with $m_{\ell\ell}$. However, beyond the peaks of γ^* -peak and Z^* -peak we have two more peaks which are

corresponding to h^0 and H in this case. In the case of $M_{A_0} = 300$ GeV, there aren't peaks of M_H since we set $M_H = 500$ GeV in the numerical analysis. At $M_{A_0} = 800$ GeV, we observe very small peak at $m_{\ell\ell} = 500$ GeV in type I because the contribution from H -pole is smaller than other ones. In the case of type II, the attribution from H -pole is enhanced by t_β . As a result, this contribution is significance in this case. Subsequently, we have a visible peak of $m_{\ell\ell} = M_H = 500$ GeV.

At high mass region of M_{A_0} , the decay rates of tree level amplitude are more significance contributions which are proportional to t_β in type II. At $M_{A_0} = 800$ GeV, one finds that decay rates are proportional to t_β in high mass regions for $m_{\ell\ell} \geq \sim 450$ GeV in THDM with type II.

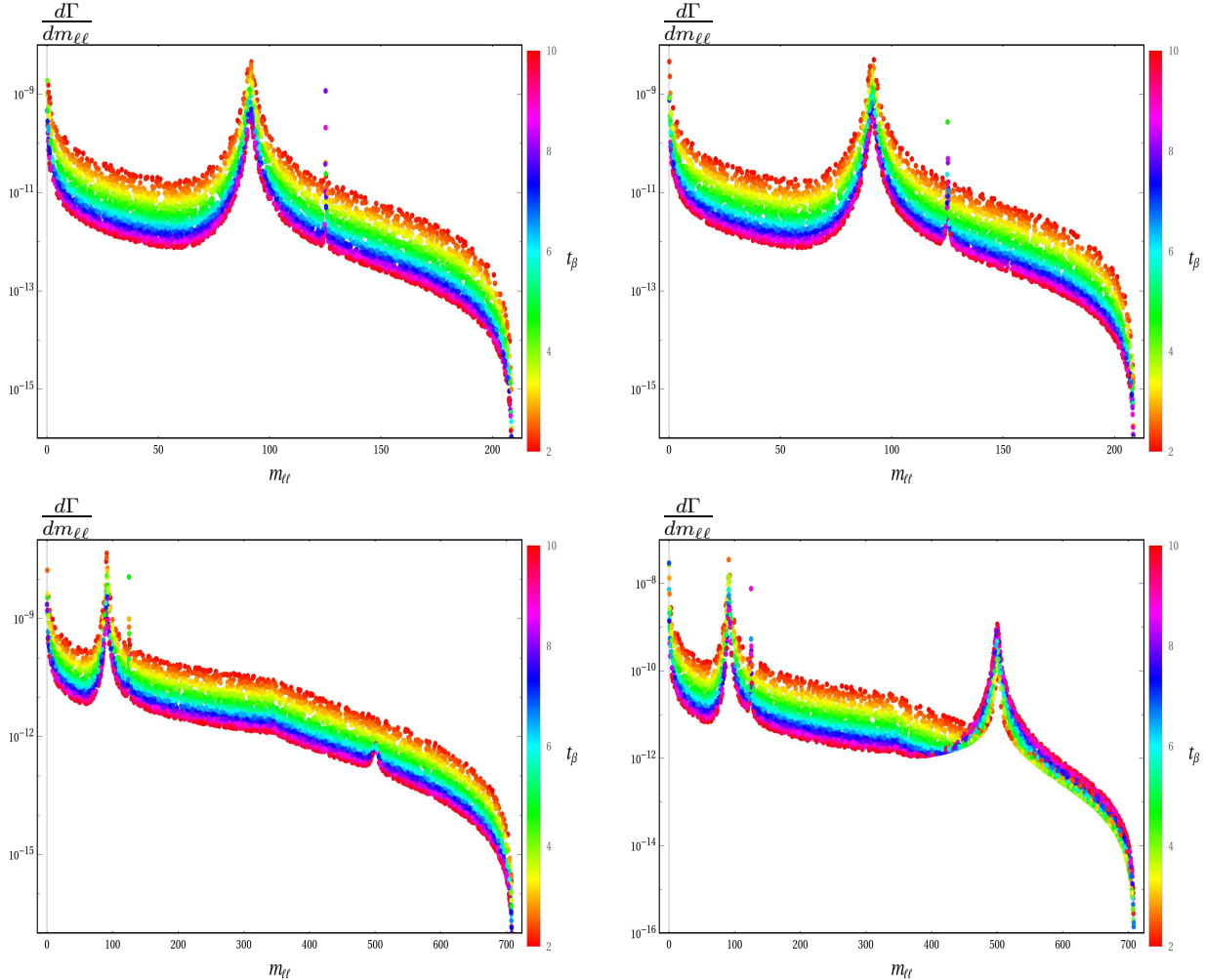


Figure 12: Differential decay rates with respect to $m_{\ell\ell}$ for $A^0 \rightarrow \ell\bar{\ell}Z$ as function of t_β in the THDM with types I and II are shown in the plots. In the left panel, we show the decay rates at $M_{A_0} = 300$ (above figure) and at 800 GeV (below figure) for the THDM with type I. We present the decay rates at $M_{A_0} = 300, 800$ GeV for the THDM with type II in the right panel, as same convention. In the plots, we vary $2 \leq t_\beta \leq 10$ and set $M_H = 500$ GeV.

4.2. THM

We next consider the phenomenological results for the THM in this paper. The constraints on the physical parameters in the THM by including the theoretical constraints as well as experimental data are first reviewed and the subjects have studied in Refs. [48, 49, 50, 51, 52, 53,

[54, 55, 56, 57, 58, 59, 61, 62, 63]. Combining all of the current constraints, we take the parameters for the THM logically as follows: $c_\alpha = 0.995$ for the alignment limit of the SM, varying $2 \leq t_{\beta^\pm} \leq 10$ and setting $M_H = 500$ GeV. The decay widths of CP-even Higgs H is calculated as in Eq. (84) with following coefficient couplings as $\kappa_H^f = c_\alpha$, $\kappa_H^V = c_\alpha c_{\beta^\pm} + \sqrt{2}s_\alpha s_{\beta^\pm}$.

4.2.1. Decay processes $A^0 \rightarrow \ell\bar{\ell}\gamma$

Total decay rates for $A^0 \rightarrow \ell\bar{\ell}\gamma$ are shown as functions of M_{A^0} in Fig. 13. In the left (and right) figure, the results for $t_{\beta^\pm} = 5$ (and $t_{\beta^\pm} = 10$) are plotted, respectively. In these plots, the red-dotted points present for tree decay rates and the blacked-dotted points are for the total decay rates. While the green-dotted points show for the decay rates from one-loop amplitude. The small figures in the corner of the corresponding plots are the absolute value of decay rates evaluating from the interference tree and one-loop amplitudes. The results of the interference tree and one-loop amplitudes can be omitted in this case. In general, the total decay rates are proportional to M_{A^0} and are slightly proportional to t_{β^\pm} .

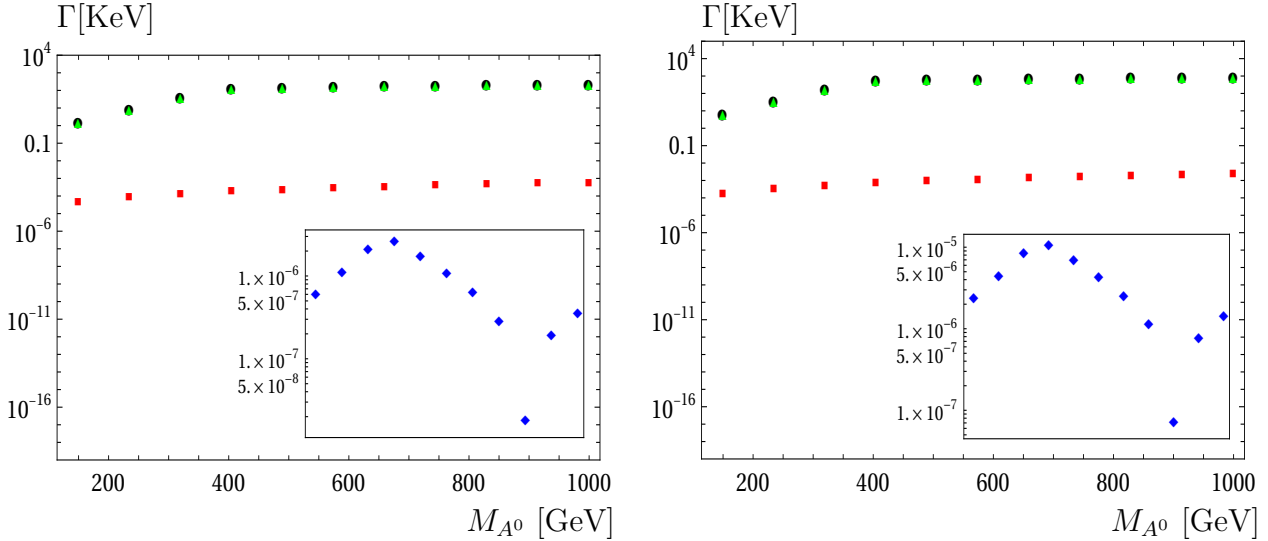


Figure 13: Total decay rates for $A^0 \rightarrow \ell\bar{\ell}\gamma$ in the THM. In the left panel, we show the decay rates at $t_\beta = 5$. We present the decay rates at $t_\beta = 10$ in the right panel. In the plots, we vary $150 \text{ GeV} \leq M_{A^0} \leq 1000 \text{ GeV}$.

We next concern the differential decay widths with respect to $m_{\ell\ell}$ for channels $A^0 \rightarrow \ell\bar{\ell}\gamma$ in the THM. In the left figure, we show the results for $M_{A^0} = 300$ GeV. While the results for $M_{A^0} = 800$ GeV are plotted in the right figure. In all cases, we vary $2 \leq t_{\beta^\pm} \leq 10$. In general, we find that the decay rates are decreased with $m_{\ell\ell}$ and proportional to t_{β^\pm} . We observe two peaks of decay rates which are from γ^* -pole and Z^* -pole. The last peak of decay rates at $m_{\ell\ell} = M_{A^0}$ because one-loop form factors in Eq. (52) are dominant when $q_{12} = m_{\ell\ell}^2 \rightarrow M_{A^0}^2$.

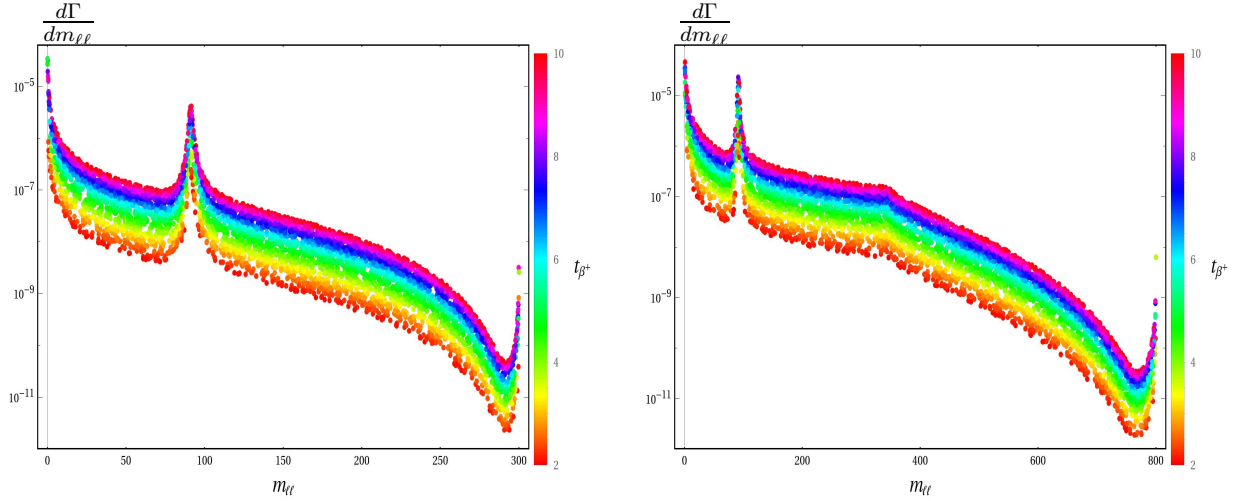


Figure 14: Differential decay rates with respect to $m_{\ell\ell}$ for $A^0 \rightarrow \ell\bar{\ell}\gamma$ as function of $t_{\beta\pm}$ in the THM. In the left panel, we show the decay rates at $M_{A^0} = 300$ GeV. We present the decay rates at $M_{A^0} = 800$ GeV for the THM in the right panel. In the plots, we vary $2 \leq t_{\beta} \leq 10$.

4.2.2. Decay processes $A^0 \rightarrow \ell\bar{\ell}Z$

Total decay rates for the processes $A^0 \rightarrow \ell\bar{\ell}Z$ in THM are presented. In the left panel, we show the decay rates at $t_{\beta+} = 5$. We present the decay rates at $t_{\beta+} = 10$ in the right panel. In these plots, we vary $150 \text{ GeV} \leq M_{A^0} \leq 1000 \text{ GeV}$. To avoid the numerical instability of the results which are from the narrow peak of the SM-like Higgs boson, one applies a cut on $q_{12} \geq q_{12}^{\min} = (M_{h_0}^2 + 1) \text{ GeV}^2$. In all plots, we use the same notations as previous cases. Two small figures in the corner of these plots are shown for decay rates of the interference between tree and one-loop amplitudes. The results indicate that these contributions are very small in comparison with other attributions and they can be ignored in this computation. In general, the total decay rates are proportional to M_{A^0} and slightly proportional to $t_{\beta\pm}$.

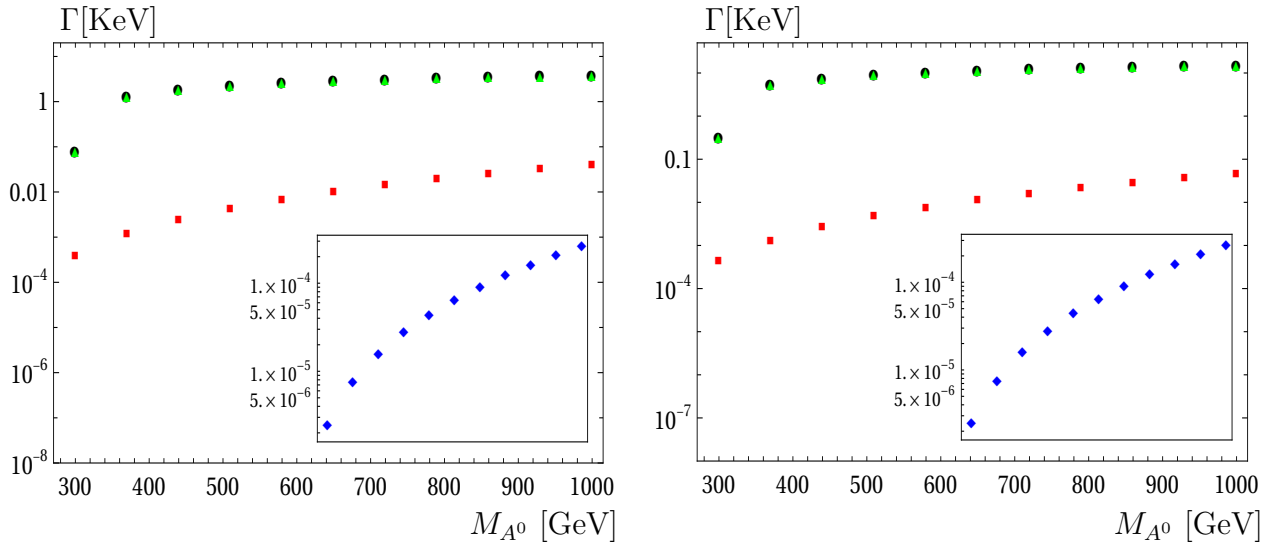


Figure 15: Total decay rates for $A^0 \rightarrow \ell\bar{\ell}Z$ in the THM. In the left panel, we show the decay rates at $t_{\beta+} = 5$. We present the decay rates at $t_{\beta+} = 10$ in the right panel. In the plots, we vary $300 \text{ GeV} \leq M_{A^0} \leq 1000 \text{ GeV}$. To avoid the numerical instability of the results, one applies a cut on $q_{12} \geq q_{12}^{\min} = (M_{h_0}^2 + 1) \text{ GeV}^2$.

Differential decay rates with respect to $m_{\ell\ell}$ are presented in Fig. 16. In the left panel, we show the decay rates at $M_{A_0} = 300$ GeV. We present the decay rates at $M_{A_0} = 800$ GeV for the THM in the right panel. In the plots, we vary $2 \leq t_{\beta\pm} \leq 10$. In general, we find that the decay rates are decreased with $m_{\ell\ell}$ and proportional to $t_{\beta\pm}$. One find two peaks corresponding to γ^* -peak and Z^* -peak in these plots. Furthermore, we also observe a narrow peak of h^0 . The peak from H give small contribution and it is invisible in these plots. As same previous cases, the decay rates develop to the peaks and decrease rapidly beyond the peaks.

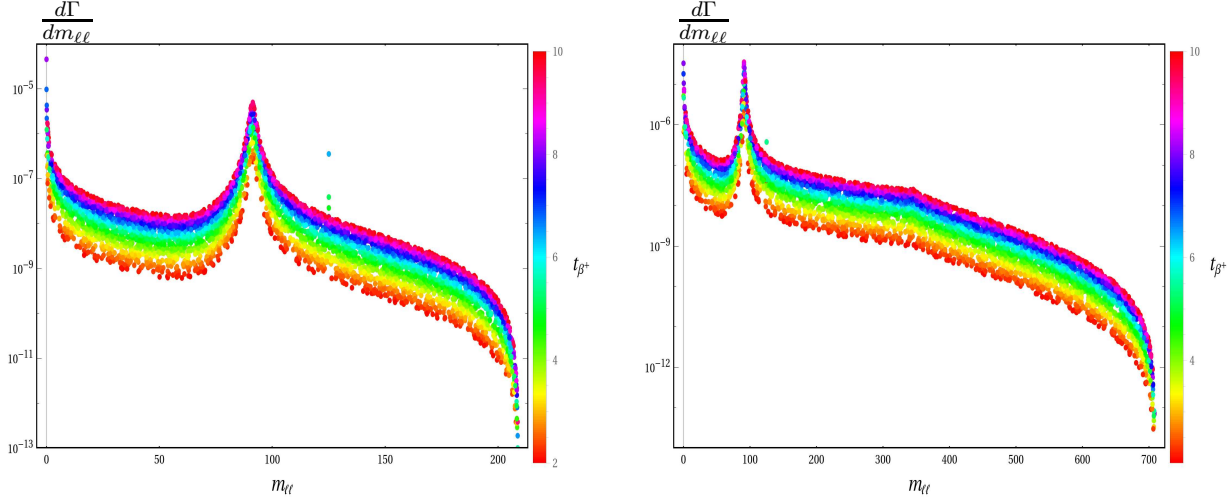


Figure 16: Differential decay rates with respect to $m_{\ell\ell}$ for $A^0 \rightarrow \ell\bar{\ell}Z$ as function of $t_{\beta\pm}$ in the THM. In the left panel, we show the decay rates at $M_{A_0} = 300$ GeV. We present the decay rates at $M_{A_0} = 800$ GeV for the THM in the right panel. In the plots, we vary $2 \leq t_{\beta\pm} \leq 10$.

5. Conclusions

In this work, we have presented a general one-loop formulas for the decay of CP-odd Higgs $A^0 \rightarrow \ell\bar{\ell}V$ with $V \equiv \gamma, Z$ within Higgs Extension Standard Models, including two higgs doublet model with a complex scalar, two higgs doublet model as well as triplet higgs model. Analytic results are expressed in terms of PV-functions following the standard notations of LoopTools. As a result, physical results can be generated numerically by using the package. In phenomenological results, we have studied the decay rates of CP-odd Higgs and the differential decay widths with respect to the invariant mass of lepton pair for all decay channel $A^0 \rightarrow \ell\bar{\ell}\gamma, \ell\bar{\ell}Z$ in THDM and THM. One finds that one-loop contributing to the decay rates and the differential decay rates are significance contributions and they should be taken into account at future colliders.

Acknowledgment: This research is funded by Vietnam National Foundation for Science and Technology Development (NAFOSTED) under the grant number 103.01-2023.16. K. H. Phan and D. T. Tran express their gratitude to all the valuable support from Duy Tan University, for the 30th anniversary of establishment (Nov. 11, 1994 - Nov. 11, 2024) towards "Integral, Sustainable and Stable Development".

Appendix A: The effective Lagrangian for STHDM

In this Appendix, we derive effective Lagrangian containing all the related couplings to the processes under consideration in STHDM. From the kinetic terms, we have

$$\begin{aligned}
\mathcal{L}_K &= (D_\mu \Phi_1)^\dagger (D_\mu \Phi_1) + (D_\mu \Phi_2)^\dagger (D_\mu \Phi_2) \\
&\supset -\frac{e}{2s_W c_W} (c_\beta \mathcal{O}_{2j} - \mathcal{O}_{1j} s_\beta) (A^0 Z_\mu \partial^\mu H_j - H_j Z_\mu \partial^\mu A^0) \\
&\quad + \frac{e}{2s_W c_W} (-s_\beta \mathcal{O}_{12} + c_\beta \mathcal{O}_{22}) (A^0 Z_\mu \partial^\mu h^0 - h^0 Z_\mu \partial^\mu A^0) \\
&\quad + \frac{1}{2} \frac{e^2 v}{s_W^2 c_W^2} [c_\beta \mathcal{O}_{1j} + s_\beta \mathcal{O}_{2j}] Z^\mu Z_\mu H_j + \frac{e M_W}{s_W} [c_\beta \mathcal{O}_{1j} + s_\beta \mathcal{O}_{2j}] W_\mu^\pm W^{\mp, \mu} H_j \\
&\quad + \frac{1}{2} \frac{e^2 v}{s_W^2 c_W^2} [c_\beta \mathcal{O}_{12} + s_\beta \mathcal{O}_{22}] Z^\mu Z_\mu h^0 + \frac{e M_W}{s_W} [c_\beta \mathcal{O}_{12} + s_\beta \mathcal{O}_{22}] W_\mu^\pm W^{\mp, \mu} h^0.
\end{aligned} \tag{67}$$

Where the rotation matrix of mixing all neutral CP-even Higgses is shown as below:

$$\mathcal{O} = \begin{pmatrix} c_{13} c_{12} & -(c_{23} s_{12} + s_{23} s_{13} c_{12}) & s_{23} s_{12} - c_{23} s_{13} c_{12} \\ c_{13} s_{12} & c_{23} c_{12} - s_{23} s_{13} s_{12} & -(s_{23} c_{12} + c_{23} s_{13} s_{12}) \\ s_{13} & s_{23} c_{13} & c_{23} c_{13} \end{pmatrix}. \tag{69}$$

The generalized Yukawa Lagrangian of STHDM is presented as follows:

$$-\mathcal{L}_Y = -\bar{Q}'_L \frac{m_u}{v_i} \tilde{\Phi}_i u_R - \bar{Q}'_L \frac{m_d}{v_j} \Phi_j d_R - \bar{L}_L \frac{m_l}{v_k} \Phi_k l_R + H.c \tag{70}$$

The four Yukawa Lagrangian types as follows

- Type I:

$$\begin{aligned}
-\mathcal{L}_Y &= -\bar{Q}'_L \frac{m_u}{v_2} \tilde{\Phi}_2 u_R - \bar{Q}'_L \frac{m_d}{v_2} \Phi_2 d_R - \bar{L}_L \frac{m_l}{v_2} \Phi_2 l_R + H.c \\
&\supset \frac{i m_u c_\beta}{v \sqrt{2} s_\beta} A^0 \bar{u}^i \gamma_5 u^i - \frac{i m_d c_\beta}{v \sqrt{2} s_\beta} A^0 \bar{d}^i \gamma_5 d^i - \frac{i m_l c_\beta}{v \sqrt{2} s_\beta} A^0 \bar{l}^i \gamma_5 l^i \\
&\quad - \frac{m_u}{v \sqrt{2} s_\beta} \mathcal{O}_{2j} H_j \bar{u}^i u^i - \frac{m_d}{v \sqrt{2} s_\beta} \mathcal{O}_{2j} H_j \bar{d}^i d^i - \frac{m_l}{v \sqrt{2} s_\beta} \mathcal{O}_{2j} H_j \bar{l}^i l^i \\
&\quad - \frac{m_u}{v \sqrt{2} s_\beta} \mathcal{O}_{22} h \bar{u}^i u^i - \frac{m_d}{v \sqrt{2} s_\beta} \mathcal{O}_{22} h \bar{d}^i d^i - \frac{m_l}{v \sqrt{2} s_\beta} \mathcal{O}_{22} h \bar{l}^i l^i.
\end{aligned} \tag{71}$$

- Type II

$$\begin{aligned}
-\mathcal{L}_Y &= -\bar{Q}'_L \frac{m_u}{v_2} \tilde{\Phi}_2 u_R - \bar{Q}'_L \frac{m_d}{v_1} \Phi_1 d_R - \bar{L}_L \frac{m_l}{v_1} \Phi_1 l_R + H.c \\
&\supset \frac{i m_u c_\beta}{v \sqrt{2} s_\beta} A^0 \bar{u}^i \gamma_5 u^i + \frac{i m_d s_\beta}{v \sqrt{2} c_\beta} A^0 \bar{d}^i \gamma_5 d^i + \frac{i m_l s_\beta}{v \sqrt{2} c_\beta} A^0 \bar{l}^i \gamma_5 l^i \\
&\quad - \frac{m_u}{v \sqrt{2} s_\beta} \mathcal{O}_{2j} H_j \bar{u}^i u^i - \frac{m_d}{v \sqrt{2} c_\beta} \mathcal{O}_{1j} H_j \bar{d}^i d^i - \frac{m_l}{v \sqrt{2} c_\beta} \mathcal{O}_{1j} H_j \bar{l}^i l^i \\
&\quad - \frac{m_u}{v \sqrt{2} s_\beta} \mathcal{O}_{22} h \bar{u}^i u^i - \frac{m_d}{v \sqrt{2} c_\beta} \mathcal{O}_{12} h \bar{d}^i d^i - \frac{m_l}{v \sqrt{2} c_\beta} \mathcal{O}_{12} h \bar{l}^i l^i.
\end{aligned} \tag{72}$$

- Type X

$$-\mathcal{L}_Y = -\bar{Q}_L \frac{m_u}{v_2} \tilde{\Phi}_2 u_R - \bar{Q}'_L \frac{m_d}{v_2} \Phi_2 d_R - \bar{L}_L \frac{m_l}{v_1} \Phi_1 l_R + H.c \quad (75)$$

$$\begin{aligned} \supset & \frac{im_u c_\beta}{v\sqrt{2}s_\beta} A^0 \bar{u}^i \gamma_5 u^i - \frac{im_d c_\beta}{v\sqrt{2}s_\beta} A^0 \bar{d}^i \gamma_5 d^i + \frac{im_l s_\beta}{v\sqrt{2}c_\beta} A^0 \bar{l}^i \gamma_5 l^i \\ & - \frac{m_u}{v\sqrt{2}s_\beta} \mathcal{O}_{2j} H_j \bar{u}^i u^i - \frac{m_d}{v\sqrt{2}s_\beta} \mathcal{O}_{2j} H_j \bar{d}^i d^i - \frac{m_l}{v\sqrt{2}c_\beta} \mathcal{O}_{1j} H_j \bar{l}^i l^i \\ & - \frac{m_u}{v\sqrt{2}s_\beta} \mathcal{O}_{22} h \bar{u}^i u^i - \frac{m_d}{v\sqrt{2}s_\beta} \mathcal{O}_{22} h \bar{d}^i d^i - \frac{m_l}{v\sqrt{2}c_\beta} \mathcal{O}_{12} h \bar{l}^i l^i. \end{aligned} \quad (76)$$

- Type Y:

$$-\mathcal{L}_Y = -\bar{Q}_L \frac{m_u}{v_2} \tilde{\Phi}_2 u_R - \bar{Q}'_L \frac{m_d}{v_1} \Phi_1 d_R - \bar{L}_L \frac{m_l}{v_2} \Phi_2 l_R + H.c \quad (77)$$

$$\begin{aligned} \supset & \frac{im_u c_\beta}{v\sqrt{2}s_\beta} A^0 \bar{u}^i \gamma_5 u^i + \frac{im_d s_\beta}{v\sqrt{2}c_\beta} A^0 \bar{d}^i \gamma_5 d^i - \frac{im_l c_\beta}{v\sqrt{2}s_\beta} A^0 \bar{l}^i \gamma_5 l^i \\ & - \frac{m_u}{v\sqrt{2}s_\beta} \mathcal{O}_{2j} H_j \bar{u}^i u^i - \frac{m_d}{v\sqrt{2}c_\beta} \mathcal{O}_{1j} H_j \bar{d}^i d^i - \frac{m_l}{v\sqrt{2}s_\beta} \mathcal{O}_{2j} H_j \bar{l}^i l^i \\ & - \frac{m_u}{v\sqrt{2}s_\beta} \mathcal{O}_{22} h \bar{u}^i u^i - \frac{m_d}{v\sqrt{2}c_\beta} \mathcal{O}_{12} h \bar{d}^i d^i - \frac{m_l}{v\sqrt{2}s_\beta} \mathcal{O}_{22} h \bar{l}^i l^i. \end{aligned} \quad (78)$$

Appendix B: The effective Lagrangian for THM

We next derive the couplings relating to the processes under consideration in the THM. From the kinematic terms, one has

$$\mathcal{L}_K = (D_\mu \Phi)^\dagger (D^\mu \Phi) + Tr[(D_\mu \Delta)^\dagger (D^\mu \Delta)] \quad (79)$$

$$\begin{aligned} \supset & \frac{e(2s_\alpha c_{\beta^0} - s_{\beta^0} c_\alpha)}{s_{2W}} (Z_\mu A^0 \partial^\mu h^0 - Z^\mu h^0 \partial_\mu A^0) + \frac{e(2c_\alpha c_{\beta^0} + s_{\beta^0} s_\alpha)}{s_{2W}} (Z_\mu A^0 \partial^\mu H - Z^\mu H \partial_\mu A^0) \\ & + \frac{e^2 v}{s_{2W}^2} (c_{\beta^0} c_\alpha + 2s_\alpha s_{\beta^0}) h^0 Z^\mu Z_\mu + \frac{v e^2}{s_{2W}^2} (-c_{\beta^0} s_\alpha + 2c_\alpha s_{\beta^0}) H Z^\mu Z_\mu \\ & + \frac{e M_W}{s_W} (c_\alpha c_{\beta^\pm} + \sqrt{2} s_\alpha s_{\beta^\pm}) h^0 W_\mu^\pm W^{\mp, \mu} + \frac{e M_W}{s_W} (-s_\alpha c_{\beta^\pm} + \sqrt{2} c_\alpha s_{\beta^\pm}) H W_\mu^\pm W^{\mp, \mu}. \end{aligned} \quad (80)$$

The Yukawa Lagrangian for THM can be expanded as follows:

$$\mathcal{L}_Y = \mathcal{L}_Y^{SM} - L_i^T y_\nu C(i\sigma^2 \Delta) L_i + H.c, \quad (81)$$

$$\begin{aligned} \supset & i \frac{s_{\beta^0} Y_l}{\sqrt{2}} (\bar{l}_L A^0 l_R - \bar{l}_R A^0 l_L) + i \frac{s_{\beta^0} Y_d}{\sqrt{2}} (\bar{d}_L A^0 d_R - \bar{d}_R A^0 d_L) - i \frac{s_{\beta^0} Y_u}{\sqrt{2}} (\bar{u}_L A^0 u_R - \bar{u}_R A^0 u_L) \\ & - \frac{c_\alpha Y_f}{\sqrt{2}} (\bar{f}_L h^0 f_R + \bar{f}_R h^0 f_L) + \frac{s_\alpha Y_f}{\sqrt{2}} (\bar{f}_L H f_R + \bar{f}_R H f_L) \end{aligned} \quad (82)$$

$$= i \frac{s_{\beta^0} Y_l}{\sqrt{2}} A^0 \bar{l}^i \gamma_5 l^i + i \frac{s_{\beta^0} Y_d}{\sqrt{2}} A^0 \bar{d}^i \gamma_5 d^i - i \frac{s_{\beta^0} Y_u}{\sqrt{2}} A^0 \bar{u}^i \gamma_5 u^i - \frac{c_\alpha Y_f}{\sqrt{2}} h^0 \bar{f} f + \frac{s_\alpha Y_f}{\sqrt{2}} H \bar{f} f. \quad (83)$$

We can collect all couplings of CP-even and CP-odd Higgs to fermion pair from the above Lagrangian.

The total decay width of CP-even Higgs H is calculated at LO as in [14]

$$\Gamma_H \approx \sum_f \frac{N_C^f M_H}{8\pi} \left(\kappa_H^f \frac{m_f}{v} \right)^2 \left(1 - \frac{4m_f^2}{M_H^2} \right)^{3/2} \quad (84)$$

$$+ \sum_{V=Z,W} \frac{M_H^3}{64\pi c_V M_V^4} \left(\kappa_H^V \frac{2M_V^2}{v} \right)^2 \left(1 - \frac{4M_V^2}{M_H^2} + \frac{12M_V^4}{M_H^4} \right) \sqrt{1 - \frac{4M_V^2}{M_H^2}}.$$

Where $c_V = 1(2)$ for $W(Z)$ respectively. The coefficient couplings $\kappa_H^f \sim c_{\beta-\alpha}$, $\kappa_H^V = c_{\beta-\alpha}$ for THDM and $\kappa_H^f = c_\alpha$, $\kappa_H^V = c_\alpha c_{\beta\pm} + \sqrt{2}s_\alpha s_{\beta\pm}$ for THM, respectively.

Appendix C: Mixing of A^0 with ϕ and A^0 with V^*

In this Appendix, we consider one-loop mixing of A^0 with ϕ and the mixing of A^0 with V_0^* . As we mention in section 3, mixing of A_0 with vector bosons V_0^* will be vanished due to the Slavnov-Taylor identity [31].

All one-loop diagrams of the mixing of A^0 with ϕ are shown in Fig. 17 in which all fermions, W boson, Goldstone boson and charged Higgs are exchanged in the loop.

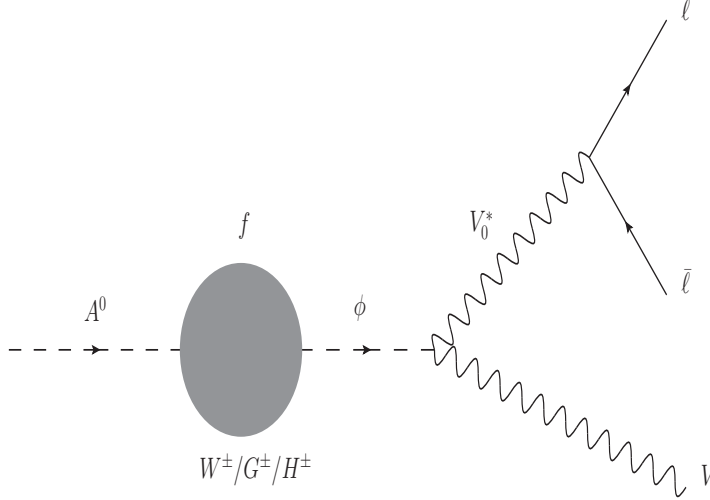


Figure 17: Group 4 One-loop self-energy Feynman diagrams mixing of A^0 with ϕ are plotted. All fermions, W boson, Goldstone boson and charged Higgs are exchanged in the loop.

The one-loop amplitude for the mixing of A_0 with ϕ is decomposed as follows:

$$\mathcal{A}_{G_4}^V = \sum_{\phi=h^0, H_j} u(q_1) \left[\mathbf{v}_{V_0^* \ell \bar{\ell}} - \mathbf{a}_{V_0^* \ell \bar{\ell}} \gamma_5 \right] \bar{v}(q_2) \frac{\left[F_{G_4, f}^{A^0 \phi} + F_{G_4, (W, \dots, H^\pm)}^{A^0 \phi} \right] \cdot \not{\epsilon}^*(q_3)}{(M_{A^0}^2 - M_\phi^2) \left[(q_{12} - M_{V_0}^2) + iM_{V_0} \Gamma_{V_0} \right]}. \quad (85)$$

One-loop form factors $F_{G_4, f}^{A^0 \phi}$ are expressed as follows:

$$F_{G_4, f}^{A^0 \phi} = -i \frac{N_C^f m_f^2}{4\pi^2} g_{\phi V_0^* V} \left\{ (\mathbf{v}_{A^0 f \bar{f}} \mathbf{v}_{\phi f \bar{f}} - \mathbf{a}_{A^0 f \bar{f}} \mathbf{a}_{\phi f \bar{f}}) A_0(m_f^2) \right.$$

$$\left. + \left[\mathbf{a}_{A^0 f \bar{f}} \mathbf{a}_{\phi f \bar{f}} M_{A^0}^2 - \mathbf{v}_{A^0 f \bar{f}} \mathbf{v}_{\phi f \bar{f}} (M_{A^0}^2 - 4m_f^2) \right] B_0(M_{A^0}^2, m_f^2, m_f^2) \right\}. \quad (86)$$

All related couplings in THDM is given by

$$\mathbf{v}_{h^0 f \bar{f}} = \frac{e}{2s_W M_W} \frac{c_\alpha}{s_\beta}, \quad \mathbf{v}_{H f \bar{f}} = \frac{e}{2s_W M_W} \frac{s_\alpha}{s_\beta}, \quad \mathbf{a}_{\phi f \bar{f}} = 0. \quad (87)$$

We verify easily that the form factor $F_{G_4, f}^{A^0 \phi}$ becomes zero because we have $\mathbf{v}_{A^0 f \bar{f}} = 0$ for CP-odd Higgs boson A^0 .

We mention the second term of G_4 involving all Feynman self-energy diagrams contributing to the mixing A^0 with ϕ with considering all vector bosons, Goldstone bosons, charged scalar particles in the loop. One-loop form factor $F_{G_4, (W, \dots, H^\pm)}^{A^0 \phi}$ is expressed in terms of scalar scalar one-loop functions as follows:

$$\begin{aligned} F_{G_4, (W, \dots, H^\pm)}^{A^0 \phi} &= -i \frac{g_\phi V_0^* V}{16\pi^2} \left\{ (g_{A^0 H^- W^+} g_{\phi H^+ W^-} + g_{A^0 H^+ W^-} g_{\phi H^- W^+}) \times \right. \\ &\quad \times \left[A_0(M_{H^\pm}^2) - 2A_0(M_W^2) + (M_W^2 - 2M_{A^0}^2 - 2M_{H^\pm}^2) B_0(M_{A^0}^2, M_{H^\pm}^2, M_W^2) \right] \\ &\quad \left. - (g_{A^0 H^- G^+} g_{\phi H^+ G^-} + g_{A^0 H^+ G^-} g_{\phi H^- G^+}) B_0(M_{A^0}^2, M_{H^\pm}^2, M_W^2) \right\}. \end{aligned} \quad (88)$$

We note that one-loop form factors $F_{G_4, (W, \dots, H^\pm)}^{A^0 \phi}$ tend zero by replacing the corresponding couplings in THDM:

$$g_{A^0 H^- W^+} \equiv g_{A^0 H^+ W^-} = \frac{e}{2s_W}, \quad (89)$$

$$g_{h^0 H^+ W^-} \equiv -g_{h^0 H^- W^+} = -\frac{e}{2s_W} c_{\beta-\alpha}, \quad (90)$$

$$g_{HH^+ W^-} \equiv -g_{HH^- W^+} = \frac{e}{2s_W} s_{\beta-\alpha}, \quad (91)$$

$$g_{A^0 H^- G^+} \equiv -g_{A^0 H^+ G^-} = \frac{e}{2s_W M_W} (M_{A^0}^2 - M_{H^\pm}^2), \quad (92)$$

$$g_{h^0 H^+ G^-} \equiv g_{h^0 H^- G^+} = \frac{e}{2s_W M_W} (M_{h^0}^2 - M_{H^\pm}^2) c_{\beta-\alpha}, \quad (93)$$

$$g_{HH^+ G^-} \equiv g_{HH^- G^+} = -\frac{e}{2s_W M_W} (M_H^2 - M_{H^\pm}^2) s_{\beta-\alpha}. \quad (94)$$

Appendix D: Mixing of V with ϕ

We next consider the mixing of V with ϕ . All self-energy diagrams contributing to the mixing of V with ϕ are shown in Fig. 18.

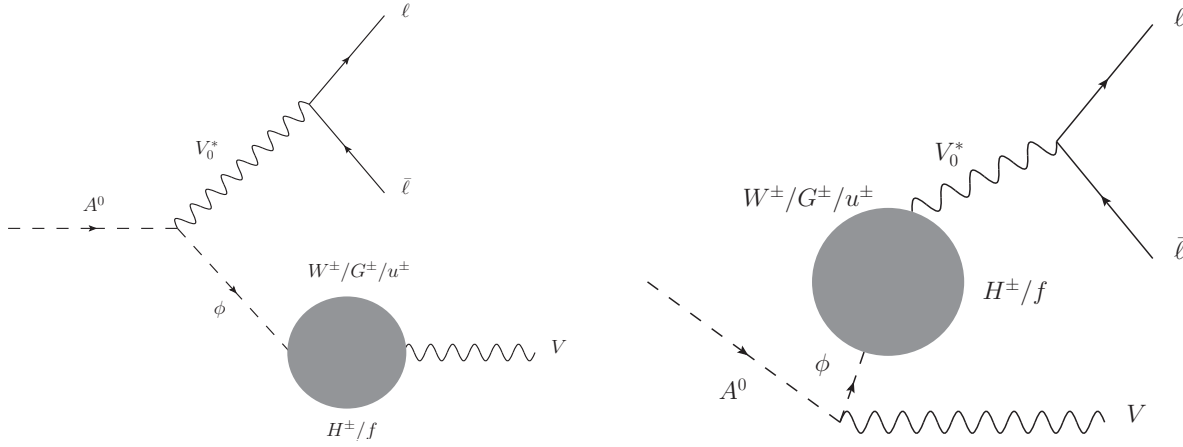


Figure 18: Group 5 One-loop Feynman diagrams for the mixing of V with ϕ .

Self-energy Feynman diagrams for one-loop CP-even Higgs boson ϕ mixing with external vector boson V , the amplitude is decomposed as follows:

$$\mathcal{A}_{G_5}^V = \sum_{\phi=h^0, H_i} \sum_{V_0=\gamma, Z} u(q_1) \left(\mathbf{a}_{V_0^* \ell \bar{\ell}} \gamma_5 \right) \bar{v}(q_2) \times \frac{\left[\sum_{f/W^\pm/H^\pm} F_{G_5, f/W^\pm/H^\pm}^{(V, \phi)}(p \cdot \epsilon^*(q_3)) \right]}{(M_V^2 - M_\phi^2) \left[(q_{12} - M_{V_0}^2) + i M_{V_0} \Gamma_{V_0} \right]}. \quad (95)$$

One-loop form factors are expressed as follows

$$F_{G_5, f}^{(V, \phi)} = \frac{-i N_f^C(m_\ell m_f^2)}{\pi^2} g_{\phi A^0 V_0^*} \times \left[(\mathbf{a}_{\phi f \bar{f}} \mathbf{a}_{V f \bar{f}} - \mathbf{v}_{\phi f \bar{f}} \mathbf{v}_{V f \bar{f}}) B_0(M_V^2, m_f^2, m_f^2) - 2 \mathbf{v}_{\phi f \bar{f}} \mathbf{v}_{V f \bar{f}} B_1(M_V^2, m_f^2, m_f^2) \right], \quad (96)$$

$$F_{G_5, H^\pm}^{(V, \phi)} = \frac{-i m_\ell}{4\pi^2} [g_{\phi A^0 V_0^*} \cdot g_{\phi H^\pm H^\mp} \cdot g_{V H^\pm H^\mp}] [B_0 + 2B_1](M_V^2, M_{H^\pm}^2, M_{H^\pm}^2), \quad (97)$$

$$F_{G_5, W^\pm}^{(V, \phi)} = \frac{-i m_\ell}{4\pi^2} g_{\phi A^0 V_0^*} \left\{ (g_{\phi u^- \bar{u}^-} g_{V u^- \bar{u}^-} + g_{\phi u^+ \bar{u}^+} g_{V u^+ \bar{u}^+}) B_1(M_V^2, M_W^2, M_W^2) + [g_{\phi W^- G^+} g_{V W^+ G^-} + g_{\phi W^+ G^-} g_{V W^- G^+}] [B_0 - B_1](M_V^2, M_W^2, M_W^2) + [g_{\phi G^\pm G^\mp} g_{V G^\pm G^\mp} + 3 g_{\phi W^\pm W^\mp} g_{V W^\pm W^\mp}] [B_0 + 2B_1](M_V^2, M_W^2, M_W^2) \right\}. \quad (98)$$

Noting that the form factor $F_{G_5, f}^{(V, \phi)}$ are simplified by applying $\mathbf{a}_{\phi f \bar{f}} = 0$. The result reads

$$F_{G_5, f}^{(V, \phi)} = \frac{i(N_f^C m_\ell m_f^2)}{\pi^2} \cdot g_{\phi A^0 V} \cdot \mathbf{v}_{\phi f \bar{f}} \cdot \mathbf{v}_{V_0^* f \bar{f}} \cdot [B_0 + 2B_1](q_{12}, m_f^2, m_f^2). \quad (99)$$

The form factors become zero by using PV-functions reduction for B_1 as follows

$$B_1(k^2, m_1^2, m_2^2) = \frac{m_2^2 - m_1^2 - k^2}{2k^2} B_0(k^2, m_1^2, m_2^2) + \frac{m_1^2 - m_2^2}{2k^2} B_0(0, m_1^2, m_2^2). \quad (100)$$

For the form factor $F_{G_2, W^\pm}^{(V, \phi)}$, applying the following relations for the couplings as

$$g_{\phi WW} = -s_{\beta-\alpha}(-c_{\beta-\alpha})\frac{eM_W}{s_W}, \quad (101)$$

$$g_{\phi G^\pm G^\mp} = \frac{e}{2M_W s_W} M_\phi^2 s_{\beta-\alpha} (c_{\beta-\alpha}) = -\frac{M_\phi^2}{2M_W^2} g_{\phi WW}, \quad (102)$$

$$g_{\phi W^\pm G^\mp} = \pm \frac{e}{2s_W} s_{\beta-\alpha} (c_{\beta-\alpha}) = \mp \frac{1}{2M_W} g_{\phi W^\pm W^\mp}, \quad (103)$$

$$g_{\phi u^\pm \bar{u}^\pm} = \frac{eM_W}{2s_W} s_{\beta-\alpha} (c_{\beta-\alpha}) = \frac{1}{2} g_{\phi W^\pm W^\mp}. \quad (104)$$

The factors $F_{G_2, W^\pm}^{(V, \phi)}$ become

$$F_{G_2, W^\pm}^{(V, \phi)} = \frac{-i m_\ell}{4\pi^2} g_{\phi A^0 V} g_{\phi W^\pm W^\mp} \left\{ \frac{1}{2} [g_{V_0^* u^- \bar{u}^-} + g_{V_0^* u^+ \bar{u}^+}] B_1(q_{12}, M_W^2, M_W^2) + \frac{1}{2M_W} (g_{V_0^* W^+ G^-} - g_{V_0^* W^- G^+}) [B_0 - B_1](q_{12}, M_W^2, M_W^2) \right\},$$

These will be vanished once V_0^* being Z -boson, the remaining couplings read

$$g_{V_0^* u^\pm \bar{u}^\pm} = \pm e \frac{c_W}{s_W}, \quad (105)$$

$$g_{V_0^* W^\pm G^\mp} = e M_W \frac{s_W}{c_W}. \quad (106)$$

In the case of V_0^* being photon, the related couplings are

$$g_{V_0^* u^\pm \bar{u}^\pm} = \pm e, \quad (107)$$

$$g_{V_0^* W^\pm G^\mp} = -e M_W. \quad (108)$$

We also verify that the factors $F_{G_2, W^\pm}^{(V, \phi)} = 0$ for both $V_0^* = \gamma^*, Z^*$.

Similarly, the form factor $F_{G_2, H^\pm}^{(V, \phi)}$ is also eliminated by the relation in Eq. (100).

References

- [1] A. Liss *et al.* [ATLAS], [[arXiv:1307.7292](#)] [hep-ex].
- [2] [CMS], [[arXiv:1307.7135](#)] [hep-ex].
- [3] H. Baer, T. Barklow, K. Fujii, Y. Gao, A. Hoang, S. Kanemura, J. List, H. E. Logan, A. Nomerotski and M. Perelstein, *et al.* [[arXiv:1306.6352](#)] [hep-ph].
- [4] R. Dermisek and J. F. Gunion, Phys. Rev. D **81** (2010), 055001 doi:10.1103/PhysRevD.81.055001 [[arXiv:0911.2460](#)] [hep-ph].
- [5] G. Aad *et al.* [ATLAS], Phys. Lett. B **744** (2015), 163-183 doi:10.1016/j.physletb.2015.03.054 [[arXiv:1502.04478](#)] [hep-ex].
- [6] G. Aad *et al.* [ATLAS], [[arXiv:2311.04033](#)] [hep-ex].
- [7] A. M. Sirunyan *et al.* [CMS], JHEP **08** (2020), 139 doi:10.1007/JHEP08(2020)139 [[arXiv:2005.08694](#)] [hep-ex].

- [8] S. Chatrchyan *et al.* [CMS], Phys. Rev. Lett. **109** (2012), 121801 doi:10.1103/PhysRevLett.109.121801 [[arXiv:1206.6326](#) [hep-ex]].
- [9] M. Krause, M. Mühlleitner and M. Spira, Comput. Phys. Commun. **246** (2020), 106852 doi:10.1016/j.cpc.2019.08.003 [[arXiv:1810.00768](#) [hep-ph]].
- [10] P. Athron, A. Büchner, D. Harries, W. Kotlarski, D. Stöckinger and A. Voigt, Comput. Phys. Commun. **283** (2023), 108584 doi:10.1016/j.cpc.2022.108584 [[arXiv:2106.05038](#) [hep-ph]].
- [11] A. Denner, S. Dittmaier and A. Mück, Comput. Phys. Commun. **254** (2020), 107336 doi:10.1016/j.cpc.2020.107336 [[arXiv:1912.02010](#) [hep-ph]].
- [12] S. Kanemura, M. Kikuchi, K. Sakurai and K. Yagyu, Comput. Phys. Commun. **233** (2018), 134-144 doi:10.1016/j.cpc.2018.06.012 [[arXiv:1710.04603](#) [hep-ph]].
- [13] S. Kanemura, M. Kikuchi, K. Mawatari, K. Sakurai and K. Yagyu, Comput. Phys. Commun. **257** (2020), 107512 doi:10.1016/j.cpc.2020.107512 [[arXiv:1910.12769](#) [hep-ph]].
- [14] S. Kanemura, M. Kikuchi and K. Yagyu, Nucl. Phys. B **983** (2022), 115906 doi:10.1016/j.nuclphysb.2022.115906 [[arXiv:2203.08337](#) [hep-ph]].
- [15] M. Aiko, S. Kanemura, M. Kikuchi, K. Sakurai and K. Yagyu, [[arXiv:2311.15892](#) [hep-ph]].
- [16] K. H. Phan, L. Hue and D. T. Tran, PTEP **2021** (2021) no.10, 103B07 doi:10.1093/ptep/ptab121 [[arXiv:2106.14466](#) [hep-ph]].
- [17] V. Van On, D. T. Tran, C. L. Nguyen and K. H. Phan, Eur. Phys. J. C **82** (2022) no.3, 277 doi:10.1140/epjc/s10052-022-10225-z [[arXiv:2111.07708](#) [hep-ph]].
- [18] A. Kachanovich, U. Nierste and I. Nišandžić, Phys. Rev. D **101** (2020) no.7, 073003 doi:10.1103/PhysRevD.101.073003 [[arXiv:2001.06516](#) [hep-ph]].
- [19] L. T. Hue, D. T. Tran, T. H. Nguyen and K. H. Phan, PTEP **2023** (2023) no.8, 083B06 doi:10.1093/ptep/ptad106 [[arXiv:2305.04002](#) [hep-ph]].
- [20] C. W. Chiang and K. Yagyu, Phys. Rev. D **87** (2013) no.3, 033003 doi:10.1103/PhysRevD.87.033003 [[arXiv:1207.1065](#) [hep-ph]].
- [21] R. Benbrik, M. Boukidi, M. Ouchemhou, L. Rahili and O. Tibsirte, Nucl. Phys. B **990** (2023), 116154 doi:10.1016/j.nuclphysb.2023.116154 [[arXiv:2211.12546](#) [hep-ph]].
- [22] A. G. Akeroyd, A. Arhrib and C. Dove, Phys. Rev. D **61** (2000), 071702 doi:10.1103/PhysRevD.61.071702 [[arXiv:hep-ph/9910287](#) [hep-ph]].
- [23] A. G. Akeroyd, A. Arhrib and M. Capdequi Peyranere, Phys. Rev. D **64** (2001), 075007 [erratum: Phys. Rev. D **65** (2002), 099903] doi:10.1103/PhysRevD.65.099903 [[arXiv:hep-ph/0104243](#) [hep-ph]].
- [24] J. Yin, W. G. Ma, R. Y. Zhang and H. S. Hou, Phys. Rev. D **66** (2002), 095008 doi:10.1103/PhysRevD.66.095008
- [25] A. Arhrib, Phys. Rev. D **67** (2003), 015003 doi:10.1103/PhysRevD.67.015003 [[arXiv:hep-ph/0207330](#) [hep-ph]].

- [26] T. Farris, J. F. Gunion, H. E. Logan and S. f. Su, Phys. Rev. D **68** (2003), 075006 doi:10.1103/PhysRevD.68.075006 [[arXiv:hep-ph/0302266](#) [hep-ph]].
- [27] K. Sasaki and T. Uematsu, Phys. Lett. B **781** (2018), 290-294 doi:10.1016/j.physletb.2018.04.005 [[arXiv:1712.00197](#) [hep-ph]].
- [28] H. Abouabid, A. Arhrib, R. Benbrik, J. El Falaki, B. Gong, W. Xie and Q. S. Yan, JHEP **05** (2021), 100 doi:10.1007/JHEP05(2021)100 [[arXiv:2009.03250](#) [hep-ph]].
- [29] W. Bernreuther, L. Chen and Z. G. Si, JHEP **07** (2018), 159 doi:10.1007/JHEP07(2018)159 [[arXiv:1805.06658](#) [hep-ph]].
- [30] E. Accomando, M. Chapman, A. Maury and S. Moretti, Phys. Lett. B **818** (2021), 136342 doi:10.1016/j.physletb.2021.136342 [[arXiv:2002.07038](#) [hep-ph]].
- [31] M. Aiko, S. Kanemura and K. Sakurai, Nucl. Phys. B **986** (2023), 116047 doi:10.1016/j.nuclphysb.2022.116047 [[arXiv:2207.01032](#) [hep-ph]].
- [32] A. G. Akeroyd, S. Alanazi and S. Moretti, J. Phys. G **50** (2023) no.9, 095001 doi:10.1088/1361-6471/ace3e1 [[arXiv:2301.00728](#) [hep-ph]].
- [33] W. Esmail, A. Hammad and S. Moretti, JHEP **11** (2023), 020 doi:10.1007/JHEP11(2023)020 [[arXiv:2305.13781](#) [hep-ph]].
- [34] T. Biekötter, S. Heinemeyer, J. M. No, K. Radchenko, M. O. O. Romacho and G. Weiglein,
- [35] T. Hahn and M. Perez-Victoria, Comput. Phys. Commun. **118** (1999), 153-165.
- [36] X. M. Jiang, C. Cai, Z. H. Yu, Y. P. Zeng and H. H. Zhang, Phys. Rev. D **100** (2019) no.7, 075011 doi:10.1103/PhysRevD.100.075011 [[arXiv:1907.09684](#) [hep-ph]].
- [37] M. Muhlleitner, M. O. P. Sampaio, R. Santos and J. Wittbrodt, JHEP **03** (2017), 094 doi:10.1007/JHEP03(2017)094 [[arXiv:1612.01309](#) [hep-ph]].
- [38] S. Glaus, M. Mühlleitner, J. Müller, S. Patel and R. Santos, Phys. Lett. B **833** (2022), 137342 doi:10.1016/j.physletb.2022.137342 [[arXiv:2204.13145](#) [hep-ph]].
- [39] G. C. Branco, P. M. Ferreira, L. Lavoura, M. N. Rebelo, M. Sher and J. P. Silva, Phys. Rept. **516** (2012), 1-102 doi:10.1016/j.physrep.2012.02.002 [[arXiv:1106.0034](#) [hep-ph]].
- [40] S. Nie and M. Sher, Phys. Lett. B **449** (1999), 89-92 doi:10.1016/S0370-2693(99)00019-2 [[arXiv:hep-ph/9811234](#) [hep-ph]].
- [41] S. Kanemura, T. Kasai and Y. Okada, Phys. Lett. B **471** (1999), 182-190 doi:10.1016/S0370-2693(99)01351-9 [[arXiv:hep-ph/9903289](#) [hep-ph]].
- [42] A. G. Akeroyd, A. Arhrib and E. M. Naimi, Phys. Lett. B **490** (2000), 119-124 doi:10.1016/S0370-2693(00)00962-X [[arXiv:hep-ph/0006035](#) [hep-ph]].
- [43] I. F. Ginzburg and I. P. Ivanov, Phys. Rev. D **72** (2005), 115010 doi:10.1103/PhysRevD.72.115010 [[arXiv:hep-ph/0508020](#) [hep-ph]].
- [44] S. Kanemura, Y. Okada, H. Taniguchi and K. Tsumura, Phys. Lett. B **704** (2011), 303-307 doi:10.1016/j.physletb.2011.09.035 [[arXiv:1108.3297](#) [hep-ph]].

- [45] S. Kanemura and K. Yagyu, Phys. Lett. B **751** (2015), 289-296 doi:10.1016/j.physletb.2015.10.047 [[arXiv:1509.06060](#) [hep-ph]].
- [46] L. Bian and N. Chen, JHEP **09** (2016), 069 doi:10.1007/JHEP09(2016)069 [[arXiv:1607.02703](#) [hep-ph]].
- [47] W. Xie, R. Benbrik, A. Habjia, S. Taj, B. Gong and Q. S. Yan, Phys. Rev. D **103** (2021) no.9, 095030 doi:10.1103/PhysRevD.103.095030 [[arXiv:1812.02597](#) [hep-ph]].
- [48] E. J. Chun, H. M. Lee and P. Sharma, JHEP **11** (2012), 106 doi:10.1007/JHEP11(2012)106 [[arXiv:1209.1303](#) [hep-ph]].
- [49] C. S. Chen, C. Q. Geng, D. Huang and L. H. Tsai, Phys. Lett. B **723** (2013), 156-160 doi:10.1016/j.physletb.2013.05.007 [[arXiv:1302.0502](#) [hep-ph]].
- [50] A. Arhrib, R. Benbrik, M. Chabab, G. Moulataka, M. C. Peyranere, L. Rahili and J. Ramadan, Phys. Rev. D **84** (2011), 095005 doi:10.1103/PhysRevD.84.095005 [[arXiv:1105.1925](#) [hep-ph]].
- [51] A. Arhrib, R. Benbrik, M. Chabab, G. Moulataka and L. Rahili, JHEP **04** (2012), 136 doi:10.1007/JHEP04(2012)136 [[arXiv:1112.5453](#) [hep-ph]].
- [52] A. G. Akeroyd and S. Moretti, Phys. Rev. D **86** (2012), 035015 doi:10.1103/PhysRevD.86.035015 [[arXiv:1206.0535](#) [hep-ph]].
- [53] A. G. Akeroyd and H. Sugiyama, Phys. Rev. D **84** (2011), 035010 doi:10.1103/PhysRevD.84.035010 [[arXiv:1105.2209](#) [hep-ph]].
- [54] A. G. Akeroyd and S. Moretti, Phys. Rev. D **84** (2011), 035028 doi:10.1103/PhysRevD.84.035028 [[arXiv:1106.3427](#) [hep-ph]].
- [55] M. Aoki, S. Kanemura and K. Yagyu, Phys. Rev. D **85** (2012), 055007 doi:10.1103/PhysRevD.85.055007 [[arXiv:1110.4625](#) [hep-ph]].
- [56] S. Kanemura and K. Yagyu, Phys. Rev. D **85** (2012), 115009 doi:10.1103/PhysRevD.85.115009 [[arXiv:1201.6287](#) [hep-ph]].
- [57] M. Chabab, M. C. Peyranere and L. Rahili, Phys. Rev. D **90** (2014) no.3, 035026 doi:10.1103/PhysRevD.90.035026 [[arXiv:1407.1797](#) [hep-ph]].
- [58] Z. L. Han, R. Ding and Y. Liao, Phys. Rev. D **91** (2015), 093006 doi:10.1103/PhysRevD.91.093006 [[arXiv:1502.05242](#) [hep-ph]].
- [59] M. Chabab, M. C. Peyranère and L. Rahili, Phys. Rev. D **93** (2016) no.11, 115021 doi:10.1103/PhysRevD.93.115021 [[arXiv:1512.07280](#) [hep-ph]].
- [60] N. Haba, H. Ishida, N. Okada and Y. Yamaguchi, Eur. Phys. J. C **76** (2016) no.6, 333 doi:10.1140/epjc/s10052-016-4180-z [[arXiv:1601.05217](#) [hep-ph]].
- [61] D. K. Ghosh, N. Ghosh, I. Saha and A. Shaw, Phys. Rev. D **97** (2018) no.11, 115022 doi:10.1103/PhysRevD.97.115022 [[arXiv:1711.06062](#) [hep-ph]].
- [62] S. Ashanujjaman and K. Ghosh, JHEP **03** (2022), 195 doi:10.1007/JHEP03(2022)195 [[arXiv:2108.10952](#) [hep-ph]].

- [63] R. Zhou, L. Bian and Y. Du, JHEP **08** (2022), 205 doi:10.1007/JHEP08(2022)205 [[arXiv:2203.01561](#) [hep-ph]].
- [64] M. Aoki, S. Kanemura, M. Kikuchi and K. Yagyu, Phys. Rev. D **87** (2013) no.1, 015012 doi:10.1103/PhysRevD.87.015012 [[arXiv:1211.6029](#) [hep-ph]].
- [65] J. Haller, A. Hoecker, R. Kogler, K. Mönig, T. Peiffer and J. Stelzer, Eur. Phys. J. C **78** (2018) no.8, 675 doi:10.1140/epjc/s10052-018-6131-3 [[arXiv:1803.01853](#) [hep-ph]].
- [66] D. T. Tran, T. H. Nguyen and K. H. Phan, [[arXiv:2311.02998](#) [hep-ph]].